ENHANCING EFFECTIVENESS OF AASHTO TYPE PRESTRESSED CONCRETE BRIDGE GIRDER THROUGH FIBER REINFORCED POLYMER STRENGTHENING

by

FARZIA HAQUE

Presented to the Faculty of the Graduate School of

The University of Texas at Arlington in Partial Fulfillment

of the Requirements

for the Degree of

MASTER OF SCIENCE IN CIVIL ENGINEERING

THE UNIVERSITY OF TEXAS AT ARLINGTON

May 2014

Copyright © by Farzia Haque 2014

All Rights Reserved

Acknowledgements

I thank Dr. Nur Yazdani for his constant support and guidance throughout the past two years. I thank him for bearing with my faults and guiding me and helping me to achieve the confidence to present my research. I thank him for his constant criticism, which has given me a positive outlook towards the various problems faced during my research and strengthened my determination and confidence, without which I will not be in the position where I am right now.

I would like to express my deepest gratitude to my committee members Dr. Sahadat Hossain and Dr. Shih-Ho Chao for their constant support and encouragement. I would like to thank my friends, roommates, and classmates for their support, encouragement, and critics.

I take this opportunity to thank my parents, my husband, and my brothers for being so lovable and kind.

May 7, 2014

Abstract

ENHANCING EFFECTIVENESS OF AASHTO TYPE
PRESTRESSED CONCRETE BRIDGE GIRDER
THROUGH FIBER REINFORCED
POLYMER STRENGTHENING

Farzia Haque, MS

The University of Texas at Arlington, 2014

Supervising Professor: Nur Yazdani

Fiber-reinforced polymers (FRP) are newly used materials by structural engineers compared to concrete, steel, and wood. One area in which FRP is being used more and more is the strengthening of structurally deficient concrete bridges. FRP strengthening of the bridge girder improves flexural, shear, corrosion, seismic, and impact resistance. ACI 440 committee report outlined design procedure for flexure, shear, axial force, and combined axial and bending forces based on the available research, which are considered to be conservative and also pointed out the areas that still require research. Besides experimental, analytical, and field tests finite element analysis of FRP strengthened structural members is an important area of research. In this thesis, an AASHTO-type IV prestressed concrete girder was modeled using ANSYS 14.5 that was eventually strengthened with FRP for flexure and shear. Flexural and shear failure were studied for un-strengthened and strengthened girder, which was compared with theoretical values obtained via accepted methods of hand calculation. The results obtained from the finite element analysis demonstrate that FRP can be used as an effective strengthening technique.

Table of Contents

List of Illustrations

List of Tables

Chapter 1

Introduction

1.1 Overview

Fiber-reinforced polymers (FRP) are newly used materials by structural engineers compared to concrete, steel, and wood. These materials have certain advantages over the traditional materials such as high stiffness-to-weight and strength-to-weight ratios, corrosion resistance, and constructability. Civil engineering applications of FRP include rehabilitation or restoration of the strength of a deteriorated structural member, retrofitting or strengthening a sound structural member to resist increased loads, and correction of design or construction errors. FRP is more and more frequently being used with structural members made of reinforced concrete, prestressed concrete, and masonry.

One area in which FRP is being used more and more is the strengthening of structurally deficient concrete bridges. As is widely known, a significant percentage of the bridges in the U.S. are structurally deficient. Deficiency in bridges can be caused by design flaws, deterioration due to environmental impact, increase in service loads, and accidental impacts. Traditional techniques to strengthen structural members include externally bonded steel plates, steel or concrete jackets, and external post-tensioning (American Concrete Institute [ACI], 2008). Labor and equipment costs to install FRP systems are often lower than traditional techniques and easier to install in areas with limited access (ACI). FRP systems also provide better aesthetics in many cases.

FRP strengthening of the bridge girder improves flexural, shear, corrosion, seismic, and impact resistance. Report by ACI committee 440 (2008) provides guidance for the selection, design, and installation of FRP systems for externally strengthening concrete structures based on experimental research, analytical work, and field

applications. ACI 440 report outlined design procedure for flexure, shear, axial force, and combined axial and bending forces based on the available research, which are considered to be conservative and also pointed out the areas that still require research. Besides experimental, analytical, and field tests finite element analysis of FRP strengthened structural members is an important area of research as the use of computer software to model these members is much faster and extremely cost-effective.

1.2 Scopes and Outline of Thesis

The scope of this thesis is to model a prestressed concrete AASHTO type IV bridge girder using finite element software ANSYS, to analyze for flexural and shear strengthening with FRP, and to compare the results obtained from ANSYS with ACI 440. This study provides important information on finite element modeling and analysis procedure for FRP strengthened prestressed concrete girders. The results obtained from this study will help researchers to investigate more on practical and cost-effective design procedure for flexure and shear in case of FRP strengthening.

Chapter 2 describes the literature review that was performed on precast AASHTO-type girder bridges, strengthening of prestressed concrete bridge girders using carbon FRP, flexural and shear strengthening design considerations according to ACI 440, and finite element modeling of prestressed concrete girders. Chapter 3 discusses the finite element modeling procedure in details and validation of the model comparing with hand calculations. Chapter 4 provides the analysis results for the un-strengthened girder and FRP strengthened girders against flexure and shear. It also provides comparison of ANSYS results with ACI 440. Chapter 5 provides the summary of findings, limitations of the thesis, and scopes for future research. Finite element analysis results are provided in Appendix A, notations are provided in Appendix B, and all relevant hand calculations are provided in Appendix C.

Chapter 2

Literature Review

2.1 Introduction

The focus of this thesis is the study of AASHTO-type prestressed concrete bridge girders strengthened with FRP. The following is a literature review of this thesis discussing precast AASHTO-type girder bridges, strengthening of prestressed concrete bridge girders using carbon FRP, and finite element modeling of prestressed concrete girders.

2.2 Precast AASHTO-Type Girder Bridges

Three common structural systems that are used in most of the concrete bridges are poured-in-place T-beams, precast AASHTO-type girders, and poured-in-place multi-cell box girders (Park et al., 2002). A typical AASHTO-type girder bridge is shown in Figure 2-1 and Figure 2-2. There are six types of AASHTO precast concrete I-girders that are commonly used in concrete bridges (Figure 2-3).

Figure 2-1 Elevation of Typical AASHTO-Type Girder Bridge

Figure 2-2 AASHTO-Type Girders

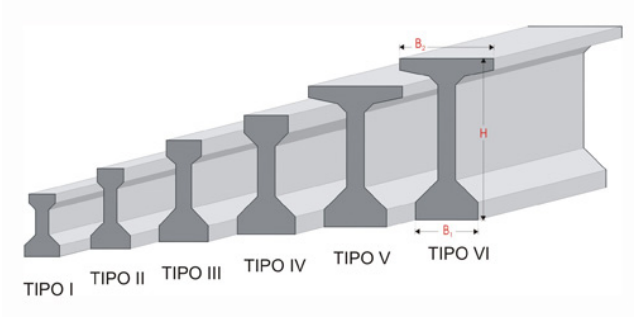

Figure 2-3 Six AASHTO-Type Girders

Flexural strengthening of AASHTO-type girders involves the addition of FRP strips to the soffit of the beam bulb as shown in Figure 2-4 (Park et al., 2002). Adequate anchorage must be provided at the ends of these strips. One form of anchorage using FRP wraps is shown in the Figure. On the other hand, for shear strengthening two alternatives can be used. Figure 2-5 shows the alternatives for FRP shear strengthening of AASHTO-type girders (Park et al., 2002). Figure 2-5a shows closed FRP stirrups, which require breaking through the top slab of the bridge and disruption to traffic. Physical restraint such as the angle and bolts are provided at the top corner of the bulb to

prevent pull away from the concrete surface. Another method is the anchorage of FRP sheets at the soffit of the top slab as shown in Figure 2-5b.

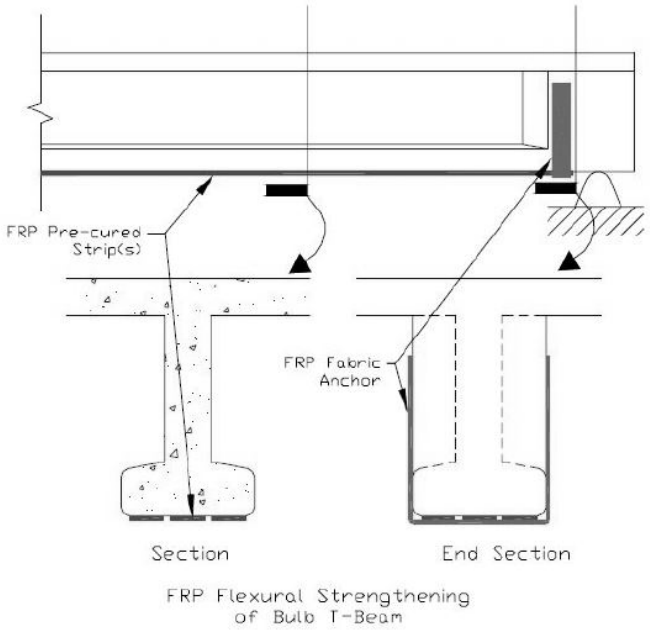

Figure 2-4 Typical Flexural Strengthening of AASHTO-Type Girder Bridge

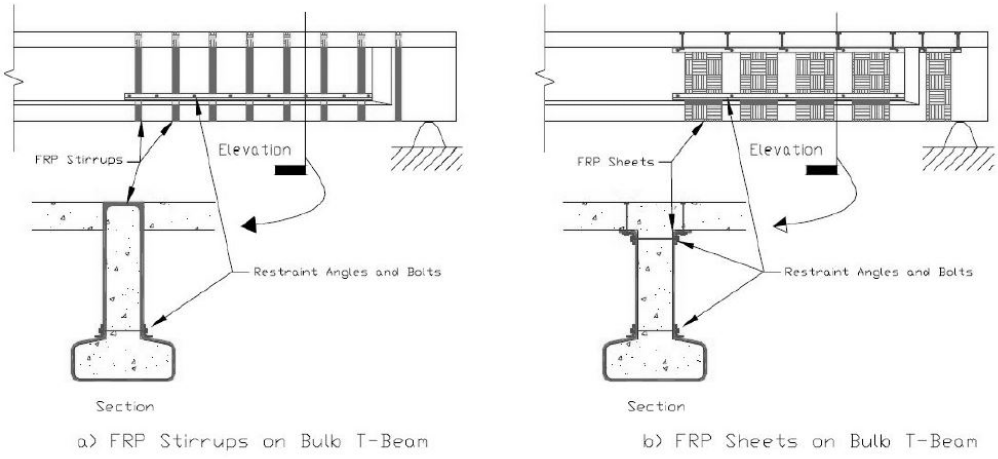

Figure 2-5 Typical Shear Strengthening of AASHTO-Type Girder Bridge

2.3 Strengthening of Prestressed Concrete Bridge Girders Using Carbon FRP

Prestressed concrete girders are the most common type of bridge girders that are used in both long and short span bridges. The prestressed girders usually deteriorate because of heavy truck load and long service life. Replacement of the prestressed concrete bridge girders generally is not economically feasible. Repair techniques to strengthen the bridge girders are very useful in terms of economy. Carbon Fiber Reinforced Polymer (CFRP) is a widely used composite material to repair prestressed concrete bridge girders. FRP is a composite material, and it is made of polymer matrix reinforced with fibers (ACI, 2011). The polymer, also known as resin, holds the fiber in place and fibers give the mechanical strength (ACI). The most common fibers that are used in civil engineering structures are glass, carbon, and aramid (ACI). Which type of fiber is used in the FRP, can be identified by modifiers; for example, glass FRP (GFRP), carbon FRP (CFRP), and aramid FRP (AFRP) (ACI). CFRP is made of fiber reinforced polymer, which is made of polymer matrix reinforced with carbon fibers. Carbon fiber is a strong, stiff, and thin fiber of nearly pure carbon, which is made by subjecting various organic raw materials to high temperatures. Although CFRP is relatively expensive, it has certain advantage including its lightweight, high tensile capacity, noncorrosive nature, conformity with the structure, strong bonding with concrete, quick applicability, and applicability to remote areas (Petty et al., 2011).

The prestressed concrete girders can be damaged or cracked due to shear force or bending moment caused by vehicular load. Experimental and analytical studies of CFRP retrofitted prestressed concrete girders showed that the use of CFRP can result in increasing moment and shear resisting capacity. The installation process of CFRP is easy and takes only few days. Strengthening of prestressed concrete girders using

CFRP helps to increase ultimate flexural capacity, enhance shear capacity, and permit easy installation without disrupting the flow of traffic.

2.3.1 Flexural Strengthening

The ultimate flexural capacity of the prestressed concrete girders can be restored using CFRP retrofit. According to Ludovico et al. (2010), the flexural capacity of prestressed concrete girders decreases as a result of loss of prestressed strands of the girders. They investigated five prestressed concrete I-shaped girders, which were designed according to ANAS (Italian Transportation Institute). One of them was undamaged, two of them were predamaged and two of them were CFRP retrofitted. Four-point loading using two hydraulic jacks was applied up to theoretical yielding. They suggested that fiber debonding between the girder and CFRP may take place in the undamaged girder, which has to be prevented to restore full flexural capacity. They found that U-wraps FRP laminates can experience 1% strains before debonding. They suggested that cementitious mortar has to be placed between concrete and repair zone to ensure perfect bonding. They concluded that both stiffness and flexural moment capacity of prestressed concrete girder can be increased by applying CFRP laminates.

Cerullo et al. (2013) conducted an investigation on a real decommissioned bridge girder repaired with externally bonded carbon-FRP. Repair of one AASHTO-type-III prestressed concrete girder was carried out from a damaged bridge and prepared for test. Before CFRP application cracks of the damaged girder were mapped and flexural behavior was examined by elastic load test. They found the shear strength deficiency of the girder by investigating the crack pattern and spalling of concrete. Horizontal cracks, caused by flexural loading, could successfully be repaired using CFRP. The Canadian Standards Association's (CSA) code was found to be conservative in design compared to conducted experiment. The CFRP retrofitting took

only three days, which was found to be very useful. Structural strengthening at a very little disruption of traffic can be effectively achieved by CFRP retrofitting. Indeed, using CFRP retrofitting technique structural strengthening of damaged prestressed concrete bridge girders can be achieved in terms of both shear and flexure resistance.

2.3.2 Shear Strengthening

The shear capacity of the prestressed concrete girder can be enhanced by retrofitting with CFRP. The girders can be deficient in shear capacity, but can be strong enough to resist moment. CFRP application can give the solution in this case. The shear design of prestressed concrete girder retrofitted with CFRP is now included in American Association of State Highway and Transportation Officials (AASHTO) and American Concrete Institute (ACI) design guides. Petty et al. (2011) tested eight simply supported AASHTO I-shaped 42 years old prestressed concrete bridge girders retrofitted with CFRP for ultimate shear capacity. A single concentrated load was applied near the AASHTO critical shear load location. Load, deflection, and strains were recorded at a rate of 10 Hz. According to them, 54% of the tensile capacity of CFRP was obtained as a result of variation in cross-section of the girder. They also found that to predict the shear capacity of the AASHTO prestressed concrete girders strut-and-tie model was the most effective one. They compared ACI method with AASHTO method and concluded that AASHTO method is more accurate for shear capacity prediction of bridge girders. They found 36% increased shear capacity using vertical U-shaped strips. Thus, CFRP retrofitting can be good option to increase the shear resistance capacity of a damaged prestressed concrete bridge girder.

2.3.3 Strengthening of Girders Subjected to Impact Loads

CFRP retrofit technique for prestressed concrete bridge girders can be used when the bridge is subjected to continuous vehicular load. Wang et al. investigated

reinforced concrete girders strengthened with CFRP under simulated vehicle loading during installation and curing (2013). Eight rectangular reinforced concrete beams of identical size and span were built in two batches. To ensure flexural response enough shear reinforcement was provided. Using control beams ultimate capacities of the beams due to four-point loading were measured. The vehicle load was simulated by a servo-hydraulic actuator at a frequency of 1Hz. The data for applied loads and strains was recorded. In their investigation, one layer of CFRP sheet was applied to RC beams and 30-50% of the total load carrying capacity of the unstrengthened beam was applied to simulate transient loading. They monitored the strain development in the CFRP sheets while simulating transient loads and found better composite action than the unstrengthened beams. They observed that the beams strengthened under simulated transient loading had more load-carrying capacity than the beams strengthened under sustained loading. They concluded that the effect of the transient loading during CFRP cure on the ultimate performance of the composite is negligible. However, their investigation does not apply where CFRP debonding is the dominating limit state because they considered concrete crushing as dominating limit state.

The retrofit technique for prestressed concrete bridge girders using CFRP is beneficial for the reasons discussed above. The damaged bridge girders need to be examined to find out the deficiency. If the girder is deficient in shear capacity, U-wraps vertical strips of CFRP can increase the shear capacity. If the girder is deficient in flexural capacity, longitudinal strips of CFRP can increase the flexural capacity. Multilayer of CFRP application is also possible if necessary. The continuous flows of traffic during application of CFRP have little impact on the performance of the composite action. However, as CFRP composites are relatively new material, further investigations are needed to accurately understand their behavior. Although this section discusses the

strengthening and ease of CFRP retrofitting, it can also be used to improve the fire resistance, impact resistance, corrosion resistance, blast resistance, and durability of the prestressed concrete bridge girders.

2.4 Design of FRP According to ACI 440 2R-08

According to ACI 440 (2008), the design material properties for FRP are based on long term environmental exposure condition because it can reduce the tensile properties and creep-rupture and fatigue endurance. The environmental reduction factor (C_E) for various FRP systems and exposure conditions is given in Table 9.1 in ACI 440. The design ultimate tensile strength and design rupture strain are calculated using following equations:

$$f_{fu} = C_E f_{fu}^{*} \quad (2.1)$$

$$\varepsilon_{fu} = C_E f_{fu}^{*} \quad (2.2)$$

2.4.1 Flexural Strengthening for Prestressed Concrete Members

Flexural strength of a FRP strengthened section depends on the controlling failure mode of the system. According to ACI 440 (2008), following failure modes should be considered for FRP strengthened section against flexure:

Crushing of the concrete in compression before yielding of the reinforcing steel;

Yielding of the steel in tension followed by rupture of the FRP laminate;

Yielding of the steel in tension followed by concrete crushing;

Shear/tension delamination of the concrete cover (cover delamination); and

Debonding of the FRP from the concrete substrate (FRP debonding).

Concrete crushing occurs if the compressive strain in the concrete reaches its maximum strain ($\varepsilon_c = 0.003$). FRP rupture occurs if the strain in the FRP reaches its design rupture strain ($\varepsilon_f = \varepsilon_{fu}$) before concrete crushing.

The design flexural strength of prestressed concrete members is computed by the following equation.

$$\varphi M_n = \varphi\left[A_p f_{ps}\left(d_p - \frac{\beta_1 c}{2}\right) + 0.85 A_f f_{fe}\left(d_f - \frac{\beta_1 c}{2}\right)\right] \quad (2.3)$$

The strength reduction factor (φ) is determined by the degree of ductility achieved by the strengthened member.

$$\varphi = \left\{\begin{array}{c} 0.90 \; for \; \in_{ps} \geq 0.013 \\ 0.65 + \frac{0.25(\in_{ps} - 0.010)}{0.013 - 0.010} \; for \; 0.010 < \in_{ps} < 0.013 \\ 0.65 \; for \; \in_{ps} \leq 0.010 \end{array}\right\} \quad (2.4)$$

ε_{ps} is the prestressing steel strain at the nominal strength and calculated by Equation 2.5.

$$\varepsilon_{ps} = \varepsilon_{pe} + \frac{p_e}{A_c E_c}\left(1 + \frac{e^2}{r^2}\right) + \varepsilon_{pnet} \leq 0.035 \quad (2.5)$$

ε_{pe} is the effective strain in the prestressing steel after losses and ε_{pnet} is the net tensile strain in the prestressing steel beyond decompression, at the nominal strength. The value of ε_{pnet} depends on the mode of failure and is calculated by Equations 2.6 and 2.7.

$$\varepsilon_{pnet} = 0.003\left(\frac{d_p - c}{c}\right) \text{ for concrete crushing failure mode} \quad (2.6)$$

$$\varepsilon_{pnet} = \left(\in_{fe} + \in_{bi}\right)\left(\frac{d_p - c}{d_f - c}\right) \text{ for FRP rupture or debonding failure modes} \quad (2.7)$$

The existing state of strain (ε_{bi}) is calculated from elastic analysis of the existing member, considering all loads that will be on the member during the installation of the FRP system. If the beam is uncracked and the only loads acting on the girder are dead loads at the time of FRP installation, ε_{bi} can be calculated by Equation 2.8.

$$\varepsilon_{bi} = -\left[\frac{P_e}{A_c E_c}\left(1 + \frac{e y_b}{r^2}\right) + \frac{M_{DL} y_b}{E_c I_g}\right] \quad (2.8)$$

The strain of FRP accounting for debonding failure mode (ε_{fd}) is calculated by Equation 2.9.

$$\varepsilon_{fd} = 0.083\sqrt{\frac{f_c'}{n_f E_f t_f}} \leq 0.9\,\varepsilon_{fu} \quad (2.9)$$

If the debonding strain is larger than the rupture strain, debonding does not control the design of the FRP system. The effective design strain for FRP (ε_{fe}) is determined by the controlling mode of failure using Equations 2.10 and 2.11.

$$\varepsilon_{fe} = 0.003\left(\frac{d_f - c}{c}\right) - \varepsilon_{bi} \leq \varepsilon_{fd} \quad \text{for concrete crushing} \quad (2.10)$$

$$\varepsilon_{fe} = \left(\in_{pu} - \in_{pi}\right)\left(\frac{d_f - c}{d_p - c}\right) - \in_{bi} \leq \in_{fd} \text{ for prestressing steel rupture} \quad (2.11)$$

$$\text{In which } \varepsilon_{pi} = \frac{P_e}{A_p E_p} + \frac{P_e}{A_c E_c}\left(1 + \frac{e^2}{r^2}\right) \quad (2.12)$$

For the neutral axis depth selected, concrete crushing would be the failure mode if the first expression of Equation 2.10 governs. If ε_{fd} governs, then FRP rupture or debonding governs the flexural failure of the section. The stress level in the FRP is calculated by Equation 2.13.

$$f_{fe} = E_f\,\varepsilon_{fe} \quad (2.13)$$

The stress level in the prestressed steel for Grade 270 ksi steel is calculated by Equation 2.14.

$$f_{ps} = \begin{cases} 28{,}500\,\in_{ps} \; for \; \in_{ps} \leq 0.0086 \\ 270 - \frac{0.04}{\in_{ps} - 0.007} \; for \; \in_{ps} > 0.0086 \end{cases} \quad (2.14)$$

With the strain and stress level in the FRP and prestressing steel calculated for the assumed neutral axis depth (c), internal force equilibrium is checked by Equation 2.15.

$$c = \frac{A_p f_{ps} + A_f f_{fe}}{\alpha_1 f_c' \beta_1 b} \quad (2.15)$$

For concrete crushing mode of failure α_1 is taken as 0.85 and β_1 is estimated per ACI 318-05. For FRP rupture, cover delamination, or FRP debonding failure β_1 can be calculate Equation 2.16.

$$\beta_1 = \frac{4\epsilon_c' - \epsilon_c}{6\epsilon_c' - 2\epsilon_c} \quad (2.16)$$

The assumed neutral axis depth (c) is adjusted until force equilibrium is satisfied.

2.4.2 Shear Strengthening

According to ACI 440 (2008), the design shear strength of an FRP-strengthened concrete member can be determined by adding the contribution of the FRP to the contributions from the reinforcing steel and the concrete as given by Equation 2.17.

$$\varphi V_n = \varphi(V_c + V_s + \psi_f V_f) \quad (2.17)$$

The additional reduction factor ψ_f is applied to the contribution of FRP, which is recommended 0.85 for the three-sided FRP U-wrap or two-opposite-sides strengthening schemes. The shear contribution of the FRP reinforcement (V_f) to the shear strength is calculated by Equation 2.18.

$$V_f = \frac{A_{fv} f_{fe} (sin\alpha + cos\alpha) d_{fv}}{s_f} \quad (2.18)$$

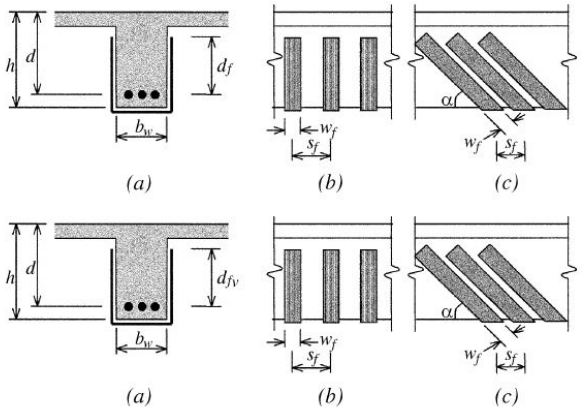

Figure 2-6 Shear Strengthening of Concrete Members (ACI 440)

The dimensions for d_{fv}, s_f, and α are shown in Figure 2-6.

The area of FRP shear reinforcement, $A_{fv} = 2nt_f w_f$ (2.19)

The effective stress in the FRP, $f_{fe} = \varepsilon_{fe} E_f$ (2.20)

The effective strain level in the FRP shear reinforcement (ε_{fe}) should be determined by considering all possible failure modes. ACI 440 outlined a procedure for determining this effective strain in case of shear strengthening of reinforced concrete members.

FRP systems that wrap two- or three-sides of the member need a bond reduction coefficient (k_v) due to the delamination from concrete before the loss of aggregate interlock. The effective strain using a bond reduction coefficient is given by Equation 2.21.

$$\varepsilon_{fe} = k_v \varepsilon_{fu} \leq 0.004 \tag{2.21}$$

The bond reduction coefficient (k_v), which is a function of concrete strength, type of wrapping scheme, and stiffness of FRP, is computed by Equation 2.22.

$$k_v = \frac{k_1 k_2 L_e}{468 \epsilon_{fu}} \leq 0.75 \tag{2.22}$$

The active bond length (L_e) is defined as the length over which majority of the bond stress is maintained. It is calculated by Equation 2.23.

$$L_e = \frac{2500}{(nt_f E_f)^{0.58}} \tag{2.23}$$

The bond reduction coefficient modification factor (k_1), which accounts for the concrete strength, is calculated by Equation 2.24.

$$k_1 = \left(\frac{f_c'}{4000}\right)^{2/3} \tag{2.24}$$

The bond reduction coefficient modification factor (k_2), which accounts for the type of wrapping scheme used, is calculated by Equation 2.25.

$$k_2 = \begin{cases} \left(\frac{d_{fv} - L_e}{d_{fv}}\right) & for\ U-wraps \\ \left(\frac{d_{fv} - 2L_e}{d_{fv}}\right) & for\ two\ sides\ bonded \end{cases} \tag{2.25}$$

The sum of total shear reinforcement provided by the steel and FRP should be limited by equation 26 based on the criteria given for steel alone in ACI 318-05.

$$V_s+V_f \leq 8\sqrt{f_c'}b_w d \quad (2.26)$$

Here it should be noted that all the equations given in this section are using in-lb units.

2.5 Finite Element Modeling

2.5.1 Finite Element Analysis

Kachlakev et al. (2001) used ANSYS to study concrete beam members externally bonded with CFRP. They modeled one quarter of the beam and finer mesh beneath the load as shown Figure 2-7. They did not model the shear reinforcement.

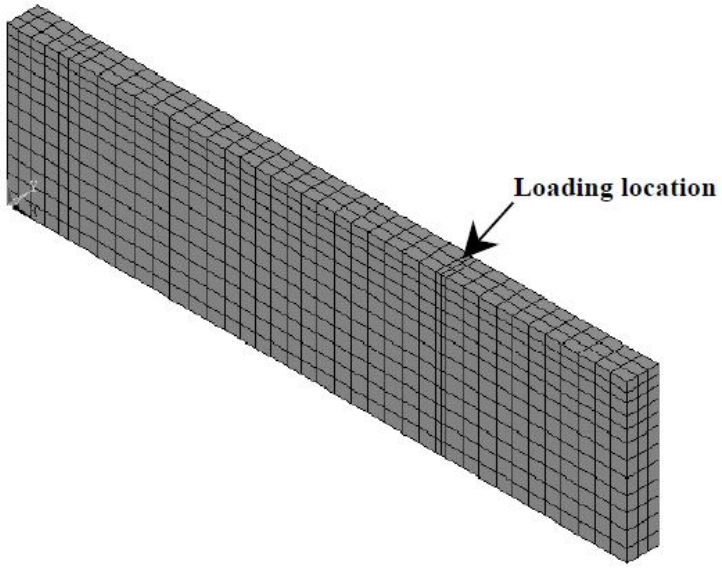

Figure 2-7 Finite Element Model for a Quarter of the Beam (Kachlakev et al., 2001)

Kachlakev et al. (2001) utilized Newton-Raphson approach to trace the equilibrium path during load-deflection response. They found that convergence of solutions for the model was difficult to achieve due to the nonlinear behavior of reinforced

concrete material. They varied the load step sizes from large (when the response was linear) to small (when concrete cracking and steel yielding occurred). They plotted load-deflection curve for unstrengthened beam, which showed reasonable correlation with experimental data as shown in Figure 2-8.

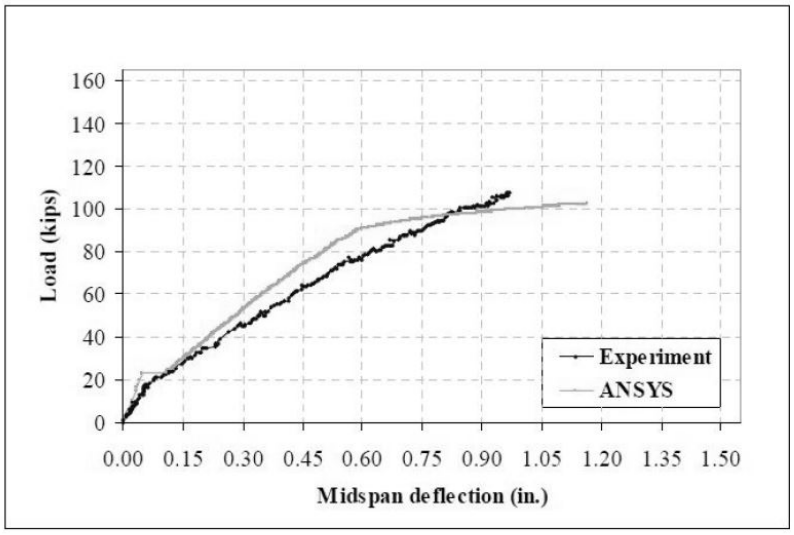

Figure 2-8 Load-deflection Plot for Control Beam (Kachlakev et al., 2001)

The ANSYS program records a crack pattern at each applied load step (Kachlakev et al., 2001). The typical cracking signs in an ANSYS model are shown in Figure 2-9. Kachlakev et al. identified three different types of concrete failure that can occur. These are flexural cracks, compression failure (crushing), and diagonal tension cracks. Flexural cracking signs, shown in the Figure 2-9 (a), appear as vertical straight lines occurring at the integration points of the concrete solid elements. Compression failures, shown in the Figure 2-9 (b), appear as circles perpendicular to the principal tensile strains at integration points in the concrete elements near the loading location. Diagonal tension cracks, shown in the Figure 2-9 (c), form as inclined lines in the beam where both normal and shear stresses act on concrete elements.

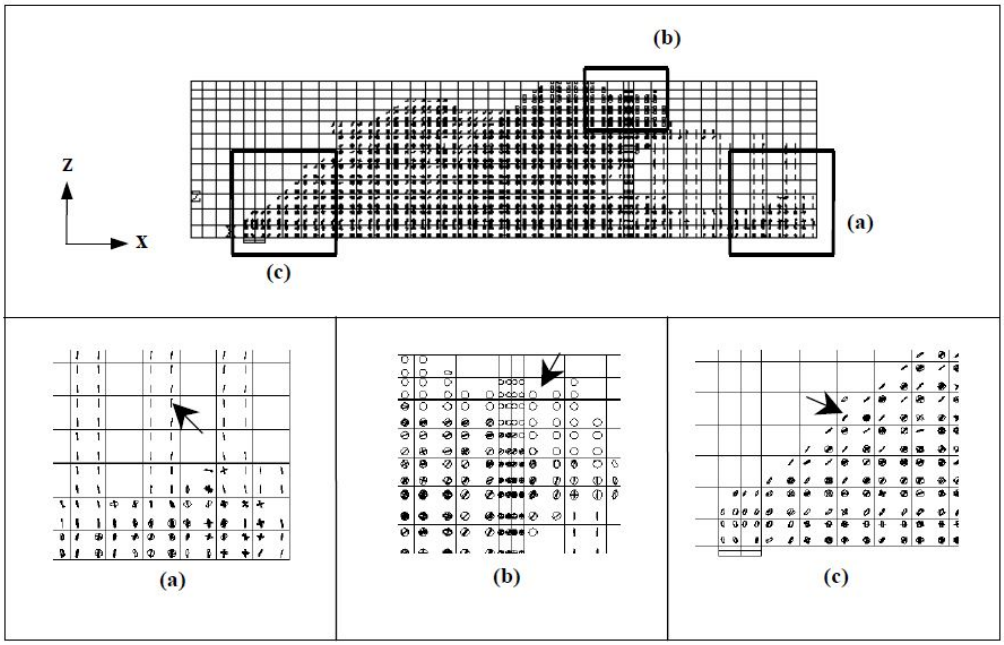

Figure 2-9 Typical Cracking Signs in Finite Element Models: (a) Flexural Cracks; (b) Compressive Cracks; and (c) Diagonal Tensile Cracks (Kachlakev et al., 2001)

2.5.2 Finite Element Modeling of Steel Reinforcement

Three techniques that are used to model steel reinforcement in the finite element models for reinforced concrete are shown in Figure 2-10 (Wolanski, 2004). These are discrete model, embedded model, and smeared model. For the discrete model bar or beam elements are used to model steel reinforcement that are connected to concrete mesh nodes. The concrete and the reinforcement mesh share the same nodes and concrete occupies the same regions occupied by the reinforcement. The drawbacks of this model are the restriction of concrete mesh by the location of reinforcement and the volume of steel reinforcement is not deducted from the concrete volume.

The embedded model overcomes the concrete mesh restriction and the stiffness of the reinforcing steel is evaluated separately from the concrete elements. This model is built in a way that keeps reinforcing steel displacements compatible with the surrounding

concrete elements. When reinforcement is complex, this model is very advantageous. However, this model increases the number of nodes and degrees of freedom in the model, which increases the run time and computational cost.

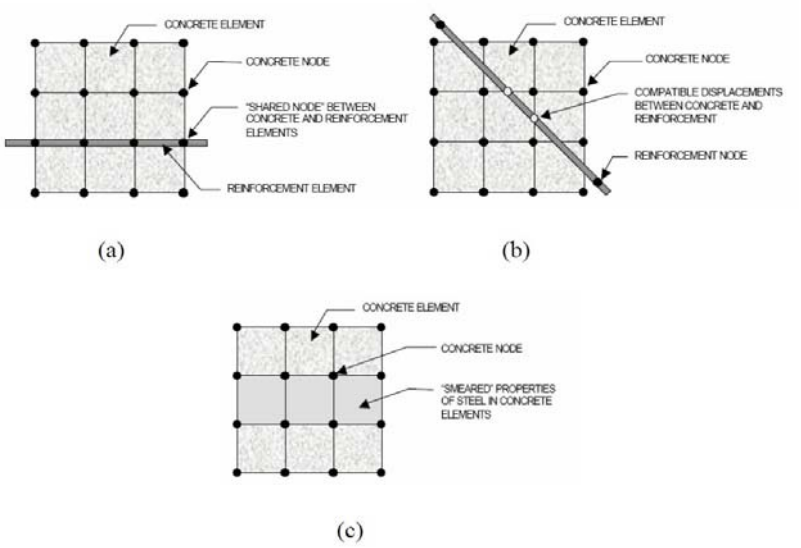

Figure 2-10 Models for Reinforcement in Reinforced Concrete: (a) Discrete; (b) Embedded; and (c) Smeared (Wolanski, 2004)

The smeared model assumes that reinforcement is uniformly spread throughout the concrete elements in a defined region of the finite element mesh. This approach is used for large-scale models where the reinforcement does not significantly contribute to the overall response of the structure.

Fanning (2001) modeled the response of the reinforcement using the discrete model and the smeared model for reinforced concrete beams and concluded that using discrete model is the best strategy when modeling reinforcement.

Chapter 3

Finite Element Modeling

ANSYS Parametric Design Language (APDL) 14.5 was used to model prestressed AASHTO I-girder. ANSYS is capable of predicting the non-linear behavior of FRP strengthened prestressed girders. A simply supported typical interior bridge beam with a span of 80 ft (24.4 m) was considered. It consists of a precast pretensioned AASHTO type IV girder. The beam was made of normal weight concrete with γ_c = 150 pcf (2402.77 kg/m^3). The mechanical properties of the precast beam were f'_c = 7000 psi (48.26 MPa); f'_{ci} = 5000 psi (34.47 MPa); E_c = 5072 ksi (34.97 GPa); E_{ci} = 4287 ksi (29.56 GPa). The prestressing tendons consist of half-inch-diameter strands with area per strand equal to 0.153 in^2 (98.71 mm^2) and strength f_{pu} = 270 ksi (1861.58 MPa).

3.1 Element Type

Three types of elements were used in the model- Solid 65, Link 180, and Shell 41. Table 3-1 shows the element types for the model.

Table 3-1 Element Types for Model

Material Type	ANSYS Element
Concrete	Solid 65
Steel Reinforcement	Link 180
Fiber Reinforced Polymer	Shell 41

Solid 65 was used to create 3-D models of concrete. This element is capable of simulating concrete cracking in tension and concrete crushing in compression. Figure 3-1 shows the element Solid 65 and its node arrangement. This element has eight nodes and three degrees of freedom at each node – translations in the nodal x, y, and z directions. This element is also capable of simulating plastic deformation and creep.

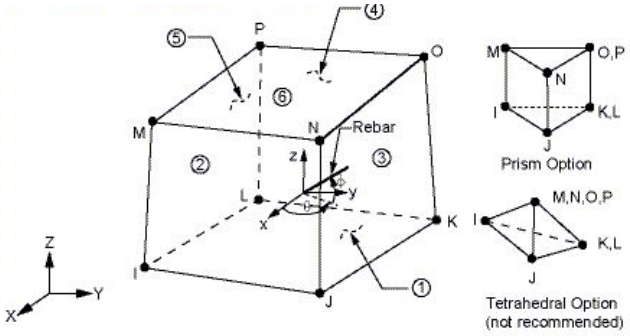

Figure 3-1 Solid 65 Geometry (ANSYS 14.5)

Element Link 180 was used model the reinforcement of the girder. Figure 3-2 shows the element Link 180 and its node arrangement. This element is a uniaxial tension-compression element. It has two nodes with three degrees of freedom at each node – translations in the nodal x, y, and z directions. This element is capable of rotation, large deflection, and large strain.

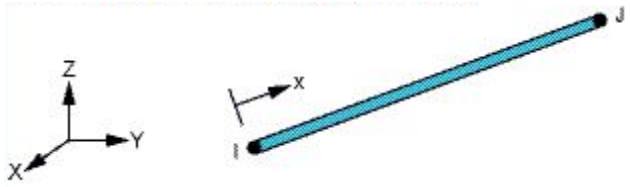

Figure 3-2 Link 180 Geometry (ANSYS 14.5)

FRP was modeled using the element Shell 41. Figure 3-3 shows Shell 41 element. This element has four nodes and each node has three degrees of freedom – translations in the nodal x, y, and z directions. Shell 41 is a 3-D element having membrane stiffness but no bending stiffness. This element has variable thickness, stress stiffening, and large deflection option.

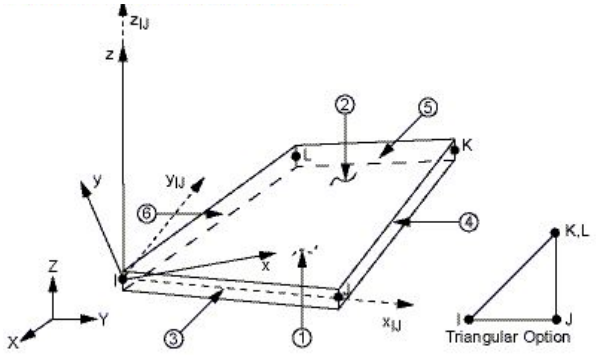

Figure 3-3 Shell 41 Geometry (ANSYS 14.5)

3.2 Real Constants

Four sets of real constants were defined for the modeling of I-girder. One was for Solid 65 element, one was for Shell 41 element, and two were for Link 180 element. Real constant set 1 was used for Solid 65 elements. In this set material numbers, volume ratio, and orientation angle value were entered zero as reinforcement was modeled as separate element.

Real constant set 2 was used for Link 180 element to represent longitudinal prestressed reinforcement with area 2.142 in^2. The mild steel rebar #3 was used as the vertical shear reinforcement in the girder. Real constant set 3 was used for Link 180 element to represent shear reinforcement with area 0.11 in^2.

Real constant set 4 was used for Shell 41 element to model epoxy. The thickness of epoxy was entered as 0.02 in.

Real constant set 5 was used for Shell 41 element to model FRP. The thickness of FRP was 0.04 in. Other parameters such as element x-axis rotation, elastic foundation stiffness, and added mass were entered as zero as they were not applicable for this model. The real constants that were used in this model are shown in Table 3-2.

Table 3-2 Real Constants for Model

Real Constant Set	Element Type	Constants			
1	Solid 65		Real Constants for Rebar 1	Real Constants for Rebar 2	Real Constants for Rebar 3
		Material Number	0	0	0
		Volume Ratio	0	0	0
		Orientation Angle	0	0	0
		Orientation Angle	0	0	0
2	Link 180	Cross-sectional Area (in^2)	2.142		
3	Link 180	Cross-sectional Area (in^2)	0.11		
4	Shell 41	Thickness (in)	0.02		
5	Shell 41	Thickness (in)	0.04		

3.3 Material Properties

The material properties for the prestressed concrete girder model were defined by 5 material models. The material models consist of concrete, mild steel rebar, prestressed steel, epoxy, and FRP. Parameters needed to define the material models are shown in Table 3-3. As shown in Table 3-3, there are multiple parts of the material model for each element.

Table 3-3 Material Models

Material Model Number	Material Type	Material Properties		
1	Concrete	Density		
		DENS	0.0002247	
		Linear Isotropic		
		EX	5072000 psi	
		PRXY	0.3	
		Multilinear Isotropic		
			Strain	Stress
		Point 1	0.000414	2099.8
		Point 2	0.0005	2455.4
		Point 3	0.001	4483.4
		Point 4	0.002	6651.4
		Point 5	0.00276	6999.4
		Point 6	0.003	7000
		Concrete		
		Open Shear Transfer Coef		0.3
		Closed Shear Transfer Coef		1
		Uniaxial Cracking Stress		627.5
		Uniaxial Crushing Stress		-1
		Biaxial Crushing Stress		0
		Hydrostatic Pressure		0
		Hydro Biax Crush Stress		0
		Hydro Uniax Crush Stress		0
		Tensile Crack Factor		0
2	Mild Steel Rebar	Linear Isotropic		
		EX	29000000 psi	
		PRXY	0.3	
		Bilinear Isotropic		
		Yield Stress	60000 psi	
		Tangent Modulus	60000 psi	
3	Prestressed Steel	Linear Isotropic		
		EX	28000000 psi	
		PRXY	0.3	
4	Epoxy	Linear Isotropic		
		EX	400000 psi	
		PRXY	0.4	

Table 3.3 - *Continued*

5	FRP	Linear Orthotropic	
		EX	9000000 psi
		EY	700000 psi
		EZ	700000 psi
		PRXY	0.22
		PRYZ	0.3
		PRXZ	0.22
		GXY	473700 psi
		GYZ	270000 psi
		GXZ	473700 psi

Material Model Number 1 refers to the Solid 65 element, which was used to model concrete. Density of the concrete was added to the material property so the self-weight of the concrete beam could be taken into account. The unit weight of the concrete was considered as 150 pcf so that density was 0.0002247 lbs^2in^{-4}. To properly model concrete the solid65 element requires linear isotropic and multilinear isotropic material properties. The multilinear isotropic material uses the Von Mises failure criterion along with the Willam and Warnke (1974) model to define the failure of the concrete. EX is the modulus of elasticity of the concrete (E_c), and PRXY is the Poisson's ratio (v). The modulus was given in the problem 5072 ksi and Poisson's ratio was assumed to be 0.3. The compressive uniaxial stress-strain relationship for the concrete model was obtained using the following equations to compute the multilinear isotropic stress-strain curve for the concrete (MacGregor 1992).

$$f = \frac{E_c * \varepsilon}{1+(\frac{\varepsilon}{\varepsilon^\circ})^2} \quad (3.1)$$

$$\varepsilon^\circ = \frac{2f_c'}{E_c} \quad (3.2)$$

$$E_c = \frac{f}{\in} \quad (3.3)$$

Where:

f = stress at any strain ε, psi

ε = strain at stress f

ε° = strain at the ultimate compressive strength f'_c

The multilinear isotropic stress-strain implemented requires the first point of the curve to be defined by the user. It must satisfy Hooke's Law;

$E = \frac{\sigma}{\varepsilon}$

The multilinear curve is used to help with convergence of the nonlinear solution algorithm.

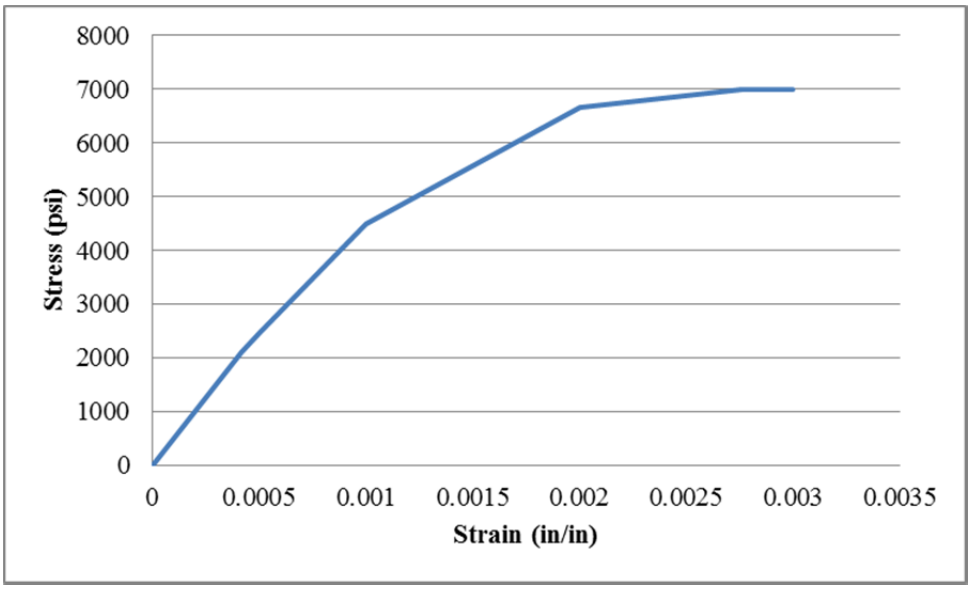

Figure 3-4 Uniaxial Stress-Strain Curve for Concrete

Figure 3-4 shows the stress-strain relationship used for this study and is based on work done by Kachlakev, et al. (2001). The first point of the graph defined as 0.30 f'_c, is calculated in the linear range. The last point is defined at f'_c and ε° = 0.003 in/in, indicating traditional crushing strain for unconfined concrete. The intermediate points were calculated using equations mentioned above. Strains were selected and the stress was calculated for each strain. Detailed of these points and calculations are shown in Appendix C.

Implementation of the Willam and Warnke (1974) material model in ANSYS requires that different constants be defined. These nine constants are:

1. Shear transfer coefficients for an open crack;
2. Shear transfer coefficients for a closed crack;
3. Uniaxial tensile cracking stress;
4. Uniaxial crushing stress (positive);
5. Biaxial crushing stress (positive);
6. Ambient hydrostatic stress state for use with constants 7 and 8;
7. Biaxial crushing stress (positive) under the ambient hydrostatic stress state (constant 6);
8. Uniaxial crushing stress (positive) under the ambient hydrostatic stress state (constant 6);
9. Stiffness multiplier for cracked tensile condition.

Typical shear transfer coefficients range from 0.0 to 1.0, with 0.0 representing a smooth crack (complete loss of shear transfer) and 1.0 representing a rough crack (no loss of shear transfer) (Wolanski, 2004). The shear transfer coefficients for open and closed cracks were determined using the work of Wolanski (2004) as a basis. The coefficient for the open crack was set to 0.3. The uniaxial cracking stress was based upon the modulus of rupture. This value is determined using,

$$f_r = 7.5^*\sqrt{f'_c}$$

The uniaxial crushing stress in this model was entered as -1 to turn off the crushing capability of the concrete element as suggested by past researchers (Wolanski, 2004). The remainders of the variables in the concrete model are left to default.

Material Model Number 2 refers to the Link 180 element. This element is being used for the shear reinforcement in the girder and it is assumed to be bilinear isotropic.

Bilinear isotropic material is also based on the Von Mises failure criteria. The bilinear model requires the yield stress (f_y), as well as the tangent modulus of the steel to be defined. The yield stress was defined as 60000 psi, and the tangent modulus was 60000 psi.

Material Model Number 3 refers to the Link 180 element. This material model is being used for the prestressing steel in the girder and it is assumed to be multilinear isotropic following the Von Mises failure criteria. The prestressing steel was modeled using a multilinear stress-strain curve developed using the following equations (Wolanski, 2004),

$\varepsilon_{ps} \leq 0.008$; $f_{ps} = 28000\ \varepsilon_{ps}$ (ksi)

$\varepsilon_{ps} > 0.008$; $f_{ps} = \left[268 - \frac{0.075}{\epsilon_{ps} - 0.0065}\right] < 0.98 f_{pu}$ (ksi)

The values entered into ANSYS for the stress-strain curve are given in Table 3.4 and Figure 3-5 shows the stress-strain behavior of the prestressing steel.

Table 3-4 Values for Multilinear Isotropic Stress-Strain Curve (Wolanski, 2004)

Strain (in/in)	Stress (ksi)	Strain (in/in)	Stress (ksi)	Strain (in/in)	Stress (ksi)	Strain (in/in)	Stress (ksi)
0	0	0.0101	247.2	0.0123	255.1	0.0145	258.6
0.008	224	0.0103	248.3	0.0125	255.5	0.0147	258.9
0.0083	226.3	0.0105	249.3	0.0127	255.9	0.0149	259.1
0.0085	230.5	0.0107	250.1	0.0129	256.3	0.0151	259.3
0.0087	233.9	0.0109	251	0.0131	256.6	0.0171	260.9
0.0089	236.8	0.0111	251.7	0.0133	257	0.0189	262
0.0091	239.2	0.0113	252.4	0.0135	257.3	0.0215	263
0.0093	241.2	0.0115	253	0.0137	257.6	0.0259	264.1
0.0095	243	0.0117	253.6	0.0139	257.9	0.0301	264.8
0.0097	244.6	0.0119	254.1	0.0141	258.1		
0.0099	245.9	0.0121	254.6	0.0143	258.4		

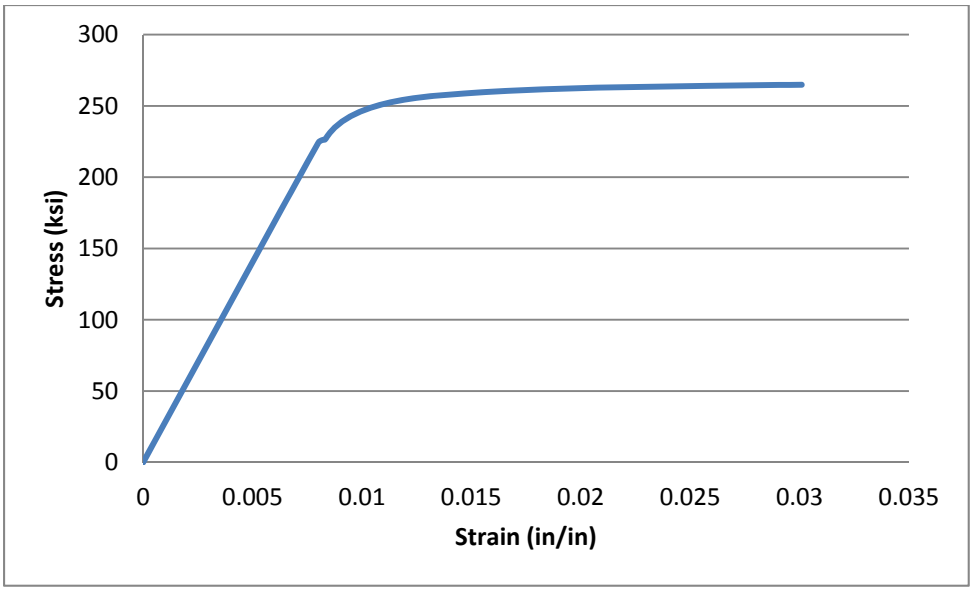

Figure 3-5 Stress-Strain Curve for 270 ksi Strand

Material Model Number 4 used to model the epoxy that connected FRP with the concrete. It was modeled as a linear isotropic material, which elastic modulus is 400000 psi and Poisson's ratio 0.3.

Material Model Number 5 used to model carbon FRP that was used to strengthen the girder. FRP was modeled using linear orthotropic material properties. Input data needed for the FRP model are as follows:

- Number of layers
- Thickness of each layer
- Orientation of the fiber direction for each layer
- Elastic modulus of the FRP in three directions (EX, EY, and EZ)
- Shear modulus of the FRP for three planes (GXY, GYZ, and GXZ)
- Major Poisson's ratio for three planes (PRXY, PRYZ, and PRXZ)

One layer of FRP was used to strengthen the girder and thickness of one layer was 0.04 in. Tensile strength of the FRP was considered as 135 ksi. Figure 3-6 shows the stress-strain curve used in this study for FRP in the direction of the fiber.

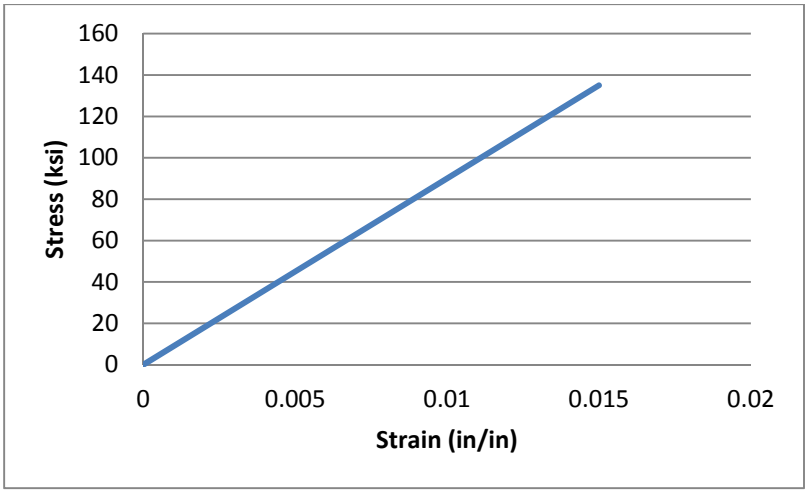

Figure 3-6 Stress-Strain Curve for FRP in the Direction of the Fibers

3.4 Modeling

AASHTO type IV girder is irregular in shape, which is not suitable to mesh and model reinforcement of the girder. To make the girder regular in shape, some conversion had been made considering its area and moment of inertia. The converted shape has same area and height as type IV girder and almost same moment of inertia. Figure 3-7 shows the actual and converted AASHTO type IV girder and Table 3-5 shows the comparison of their cross-sectional properties.

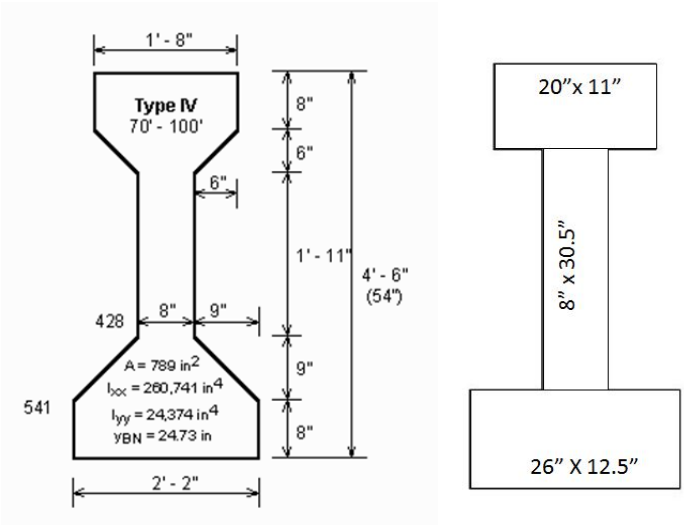

Figure 3-7 Modified AASHTO-Type IV Girder

Table 3-5 Comparisons of the Cross-sectional Properties

	Type IV	Transformed
Area, in^2	789	789
I_c, in^4	260741	262882
y, in	24.73	24.68
H, in	54	54

To model the cross-section of AASHTO-type IV girder 12 “Keypoints” were defined. Figure 3-8 shows the keypoints that were used to model the cross-section. Then the cross-sectional area was created through the keypoints. The cross-sectional area is shown in Figure 3-9.

Figure 3-8 Keypoints

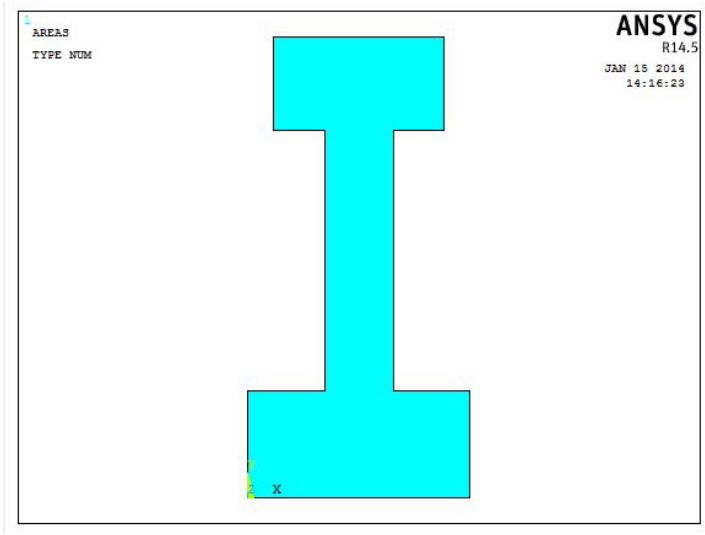

Figure 3-9 Cross-sectional Area

The cross-sectional area was meshed allowing 3 inch “edge size” using “free meshing” option. The size of the mesh was chosen based on the nodes that were needed to model reinforcement and the aspect ratio for the elements. The meshed area created 140 nodes itself. The meshed area and nodes are shown in Figure 3-10 and Figure 3-11 respectively.

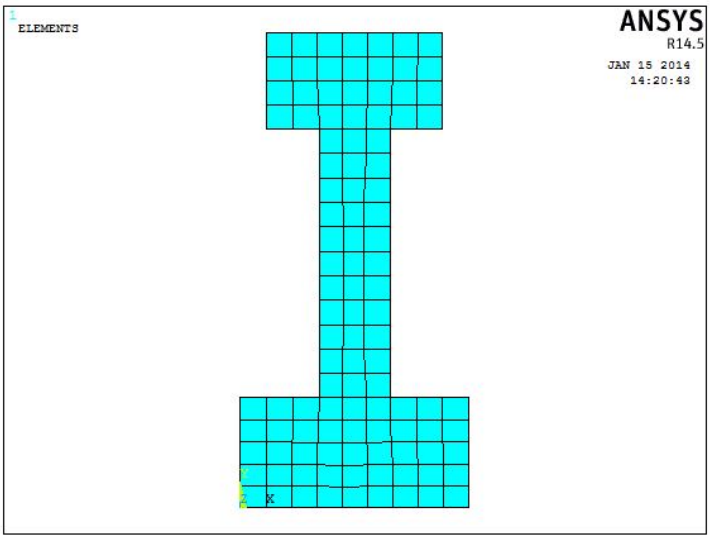

Figure 3-10 Meshed Area

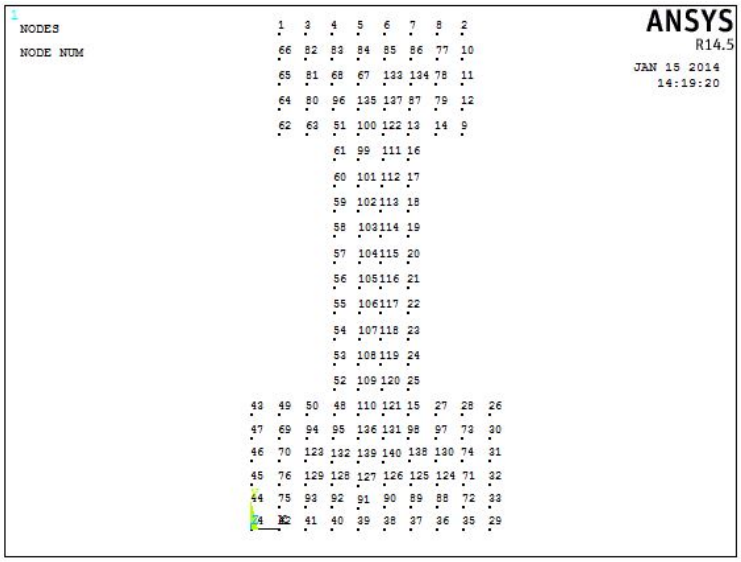

Figure 3-11 Nodes

After that, the area was extruded using Solid 65 elements for 960 inches length to model the 80ft span AASHTO type IV girder. The volume that was created by the extrusion of the cross-section is shown in Figure 3-12. The volume was divided into 53

elements along the longitudinal direction to allow for modeling the shear reinforcement. The elements for the model are shown in Figure 3-13.

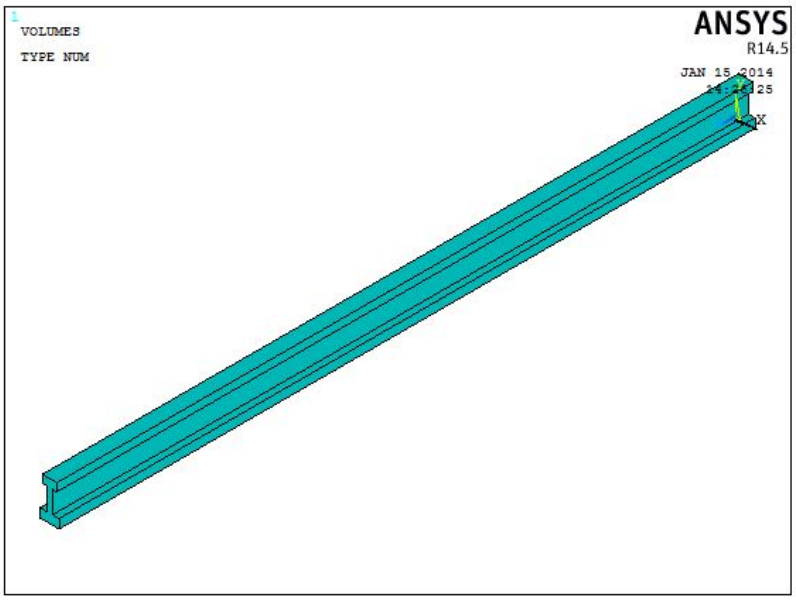

Figure 3-12 Volumes

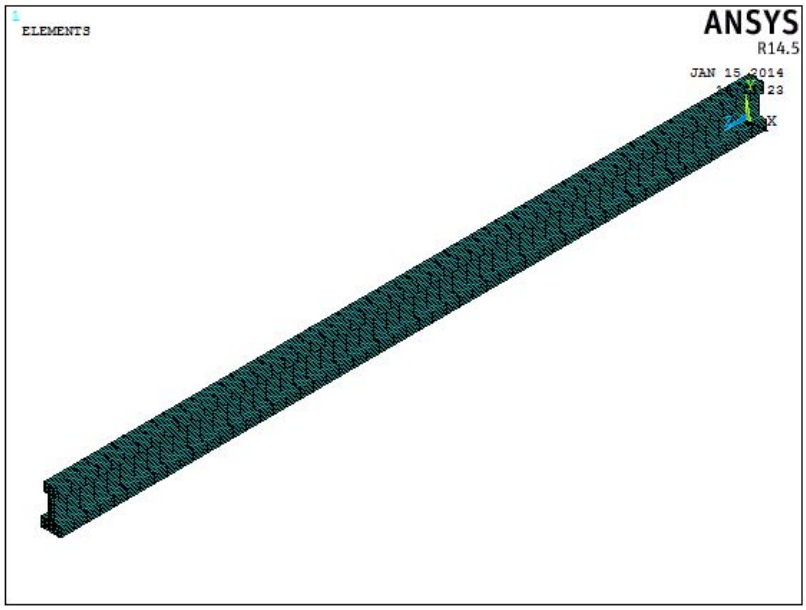

Figure 3-13 Elements

Then prestressing strands were modeled using Link 180 element, real constant set 2, and material model number 3 connecting the nodes at 5 inches from the bottom surface of the girder. The prestressing strands were modeled into two sections – one representing 14 strands. Thus total 28 strands were modeled.

Shear reinforcement was modeled at 18 in. center to center distance throughout the entire length of the girder. Link 180 element, real constant set 3, and material model number 2 were used to model shear reinforcement. Prestressing strands and shear reinforcement for the girder is shown in Figure 3-14.

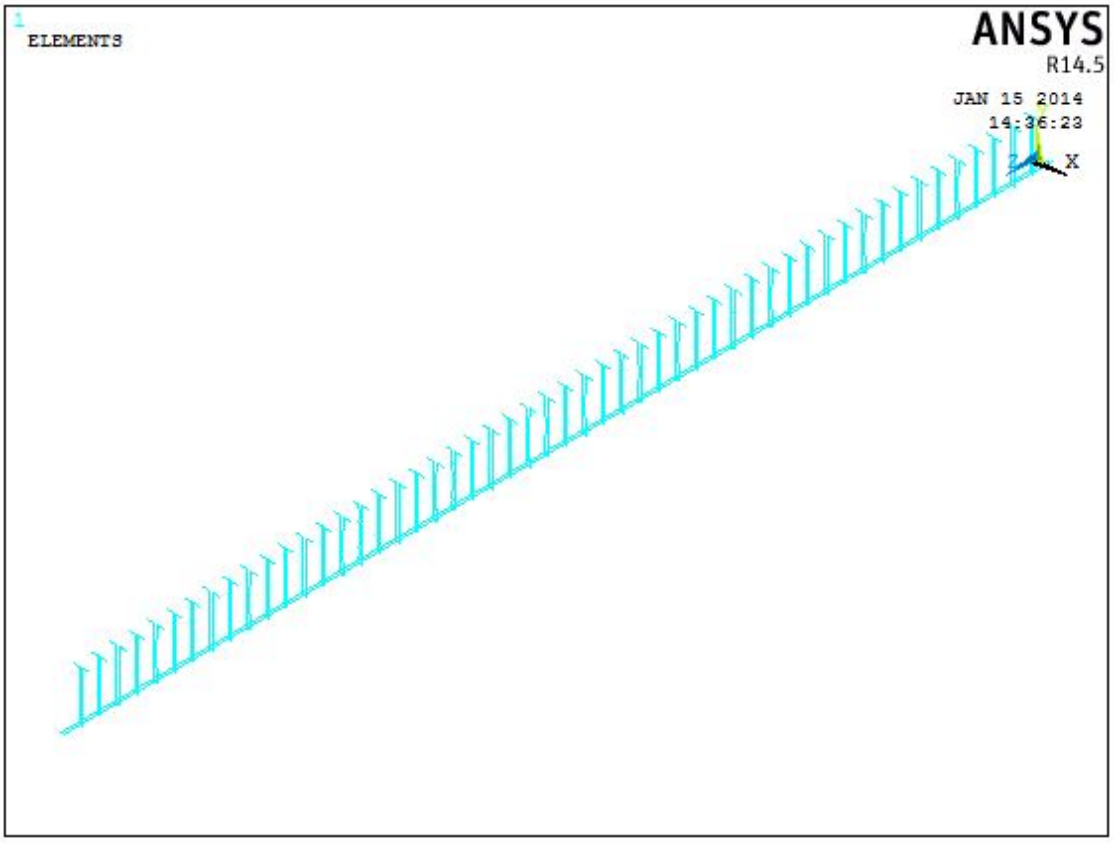

Figure 3-14 Reinforcement

To model the epoxy and the FRP a section that consists of two layers was defined – first layer for epoxy and second layer for FPR. The section properties are shown in Table 3-6. The epoxy and FRP were modeled through the nodes using the defined section. Three types of FRP configurations were used to strengthen the girder. For flexural strengthening one layer of FRP was modeled at the bottom of the girder (Figure 3-15). For shear strengthening U-wrap FRP was applied throughout the entire length of the girder as vertical and at 45 degree inclined strips (Figure 3-16).

Table 3-6 Section Lay-up for FRP

Layer	Thickness(in.)	Material Model Number
1	0.02	4
2	0.04	5

Figure 3-15 Flexural Strengthening with FRP

Figure 3-16 Shear Strengthening with FRP

3.5 Nonlinear Analysis

The finite element model for this analysis involved a simply-supported AASHTO type IV girder under transverse loading. For the purposes of this model, the static analysis was utilized. The restart command was utilized to restart an analysis after the initial run or load step had been completed. The solution controls command dictates the use of a linear or non-linear solution for the finite element model. Typical commands utilized in the nonlinear static analysis are shown in Table 3-7.

Table 3-7 Commands Used to Control Nonlinear Analysis

Analysis options	Small displacement
Calculate prestress effects	No
Time at end of loadstep	5120
Automatic time stepping	On
Number of substeps	1
Max no. of substeps	2
Min no. of substeps	1
Write Items to results file	All solution items
Frequency	Write every substep

In the particular case considered in this thesis the analysis is small displacement and static. The table shows the time at the end of the first load step. The sub steps were set to indicate load increments used for the analysis. The commands used to control the solver and outputs are shown in Table 3-8.

Table 3-8 Commands Used to Control Output

Equation solvers	Sparse direct
Number of restart file	1
Frequency	Write every substep

The commands used for the nonlinear algorithm and convergence criteria are shown in Table 3-9. The values for the convergence criteria were set to defaults except for the tolerances. The tolerances for force and displacements were set as 5 times the default values.

Table 3-9 Nonlinear Algorithm and Convergence Criteria Parameters

Line search		Off
DOF solution predictor		Program chosen
Maximum number of iteration		100
Cutback control		Cutback according to predicted number of iter.
Equiv. plastic strain		0.15
Explicit creep ratio		0.1
Implicit creep ratio		0
Incremental displacement		10000000
Points per cycle		13
Set convergence criteria		
Label	F	U
Ref. value	Calculated	Calculated
Tolerance	0.005	0.05
Norm	L2	L2
Min. ref.	Not applicable	Not applicable

Table 3-10 shows the commands used for the advanced nonlinear settings. The program behavior upon non-convergence for this analysis was set such that the program will terminate but not exit. The rest of the commands were set to defaults.

Table 3-10 Advanced Nonlinear Control Settings Used

Program behavior upon nonconvergence	Terminate but do not exit
Nodal DOF sol'n	0
Cumulative iter	0
Elapsed time	0
CPU time	0

3.6 Boundary Condition

Boundary conditions are needed to constrain the model to get a unique solution. The AASHTO-type IV girder was modeled as simply-supported. The displacement constrains were provided at the nodes of two ends. At the left end of the girder hinge support condition was modeled by applying $U_x = 0$, $U_y = 0$, and $U_z = 0$. At the right end of the girder roller support condition was modeled by applying $U_x = 0$ and $U_y = 0$. The support condition is shown in Figure 3-17.

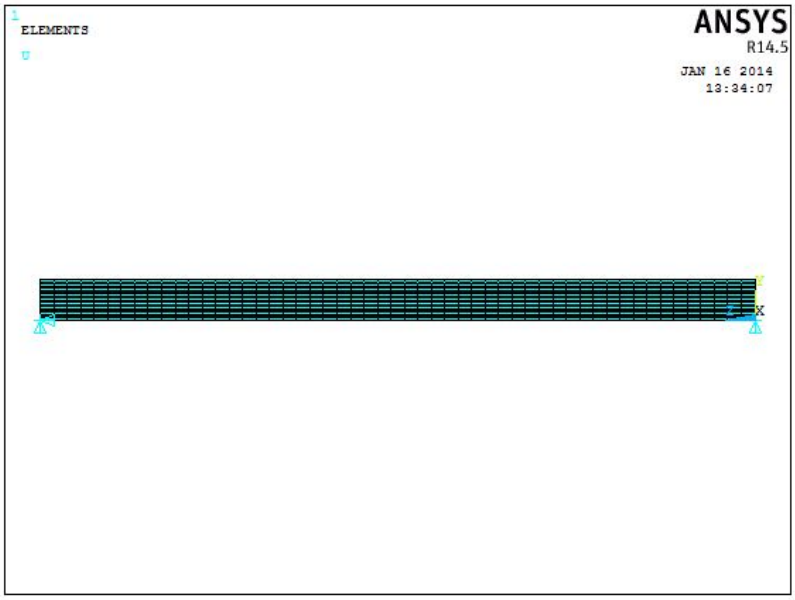

Figure 3-17 Boundary Conditions

3.7 Solution

3.7.1 Application of Prestress

In the first load step, only initial prestrain was applied. Prestressing to the strands was defined using ANSYS Command Window as there is no direct method available to provide initial strain to the link element (ANSYS, 2012). The initial strain was determined from the effective prestress (f_{pe}) and the modulus of elasticity (E_{ps}). Prestressing was defined by the following code:

inistate, set, dtyp, epel

inistate, set, mat, 3

inistate, defi, , , , , 0.003571

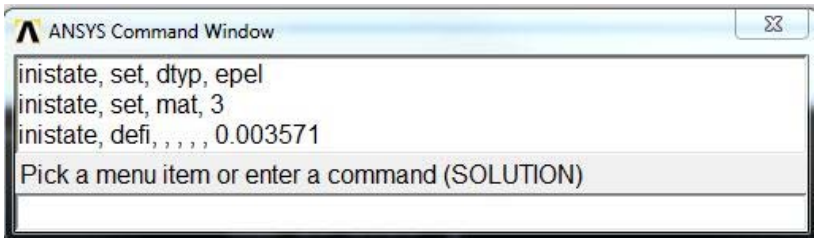

Figure 3-18 Prestressing Apply

In the above code, material refers to prestressed strands and 0.003571 is the initial strain provided in each strand. The applied prestress is therefore 99988 psi, which is low compared to practical use. It was selected based on the convergence problem that was occurring due to higher prestressing of the strands. As prestress was applied to the strands at the first load step, it produced camber. The deflected shape of the girder due to prestress is shown in Figure 3-19.

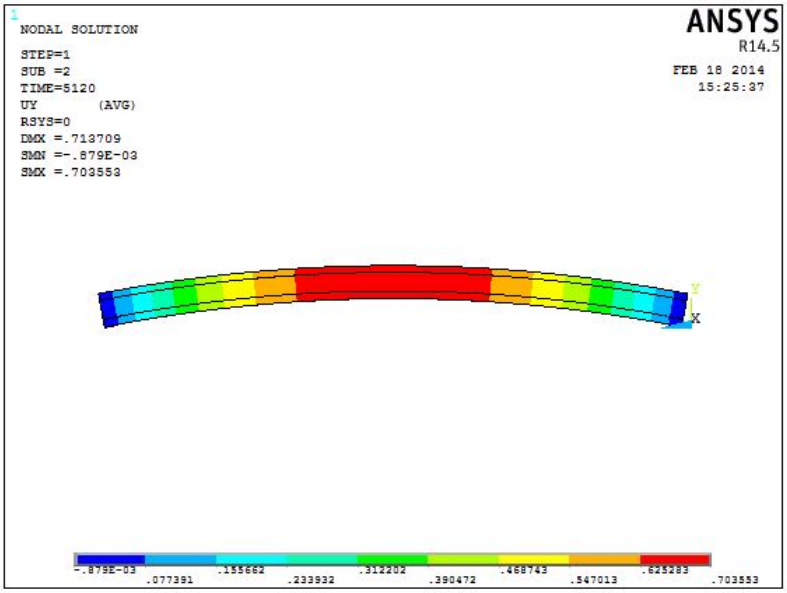

Figure 3-19 Deflection in y-Direction due to Prestress

3.7.2 Application of Self-weight

In the second load step, the self-weight of the girder was applied. The addition of the self-weight was done by applying gravitational acceleration of 386.4 in/s^2 in the global y-direction (Figure 3-20). Addition of the self-weight gave the deflected shape of the girder as shown in Figure 3-21.

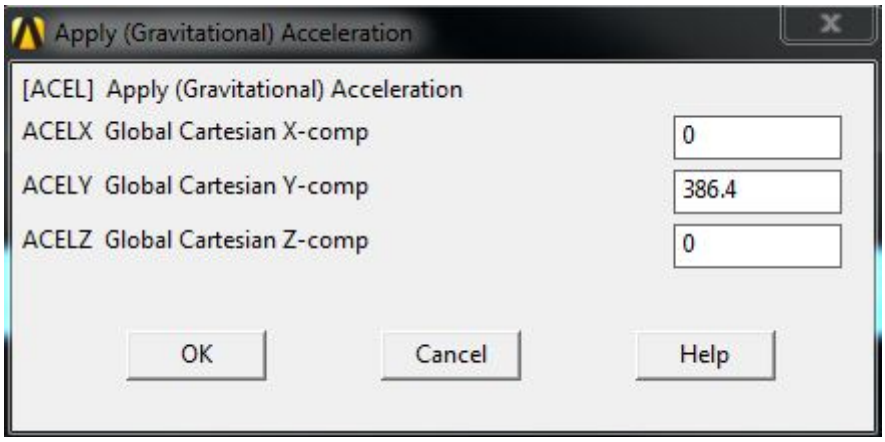

Figure 3-20 Application of Gravitational Acceleration in y-Direction

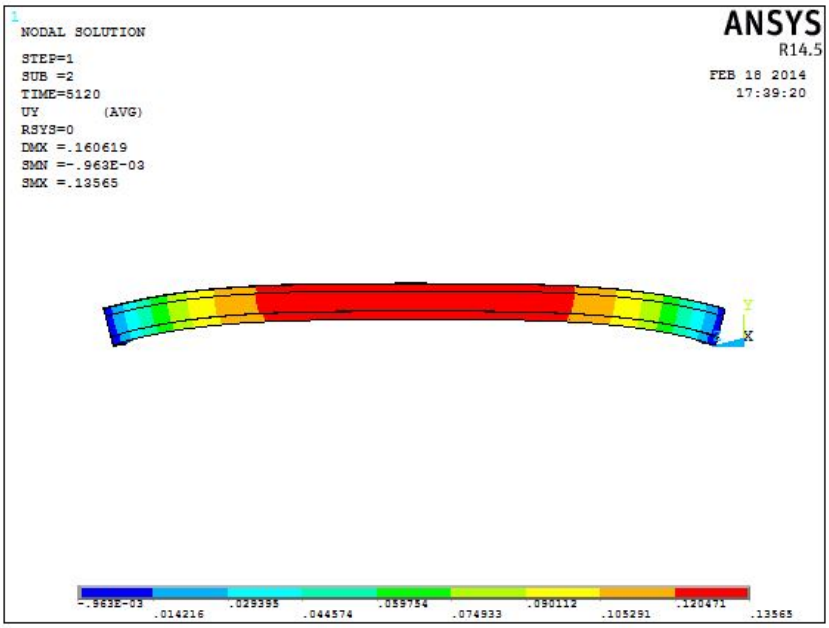

Figure 3-21 Deflection in y-Direction due to Prestress and Self-weight

3.7.3 Application of Load

The force, P, applied at the mid span of the girder. The force applied at each node was one sixteenth of the actual force applied. Figure 3-22 illustrates the applied loading. Deformed shape due to the applied load is shown in Figure 3-23.

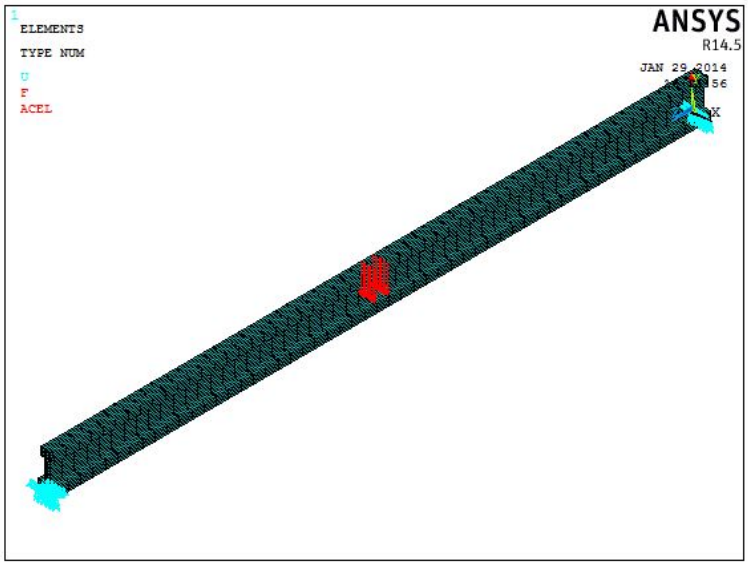

Figure 3-22 Application of External Loading

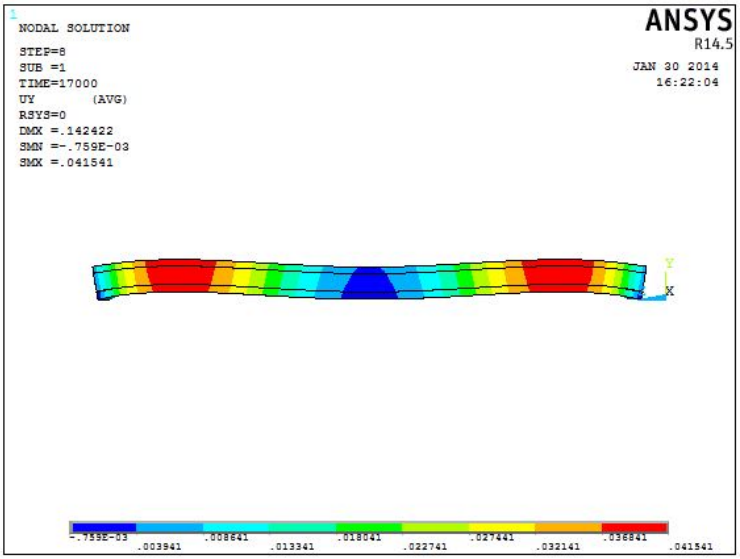

Figure 3-23 Deflection in y-Direction due to Applied Loading

3.8 Validation of the Model

The ANSYS model had been validated by comparing it to the deflection values determined by hand calculation. Both the values were close enough. The ANSYS values were slightly less than that of hand calculation. Hand calculated defections are shown in Appendix C. Table 3-11 shows comparison of ANSYS and hand calculated deflection values.

Table 3-11 Analytical Results

	ANSYS	Hand Calculations
Deflection due to Prestress (in)	-0.7036	-0.7283
Deflection at Application of Self-weight (in)	-0.1357	-0.1601

Chapter 4

Analysis and Results

4.1 Analysis Process for the Finite Element Model

The finite element analysis of the model was set up to examine three different behaviors: initial cracking of the girder, yielding of the prestressing steel, and the strength limit state of the girder. The Newton-Raphson method of analysis was used to compute the nonlinear response.

The application of the loads up to failure was done incrementally. After each load increment was applied, the restart option was used to go to the next step after convergence. The first load step taken was to produce the camber in the girder due to prestress. The second load step was the addition of the self-weight. From that point on, incremental load was applied up to the failure of the girder. A listing of the load steps, sub steps, and loads applied per restart file are shown in Table A.1 in Appendix A.

When the analysis reached the point of initial cracking, the force convergence criteria was dropped, and the reference value of the displacement criteria was 5. From this point, the load increments were decreased to capture the initial cracking of the girder. When yielding of the steel occurred, the load increments were decreased to 80 lbs. Finally, load increments were decreased to 32 lb. until unresolvable convergence failure of the nonlinear algorithm occurred.

4.2 Results

4.2.1 Unstrengthened Prestressed Girder

The analysis results showed that the load-deflection curve had seven distinct points due to the application of prestress and load increments. As seen in Figure 4-1, these distinct points are effective prestress, addition of self-weight, zero deflection, decompression, initial cracking, steel yielding, and failure.

Calculations of the effective prestress for the girder can be found in Appendix C. The comparisons between hand calculations and finite element analysis due to the prestress force are shown in Table 4-1.

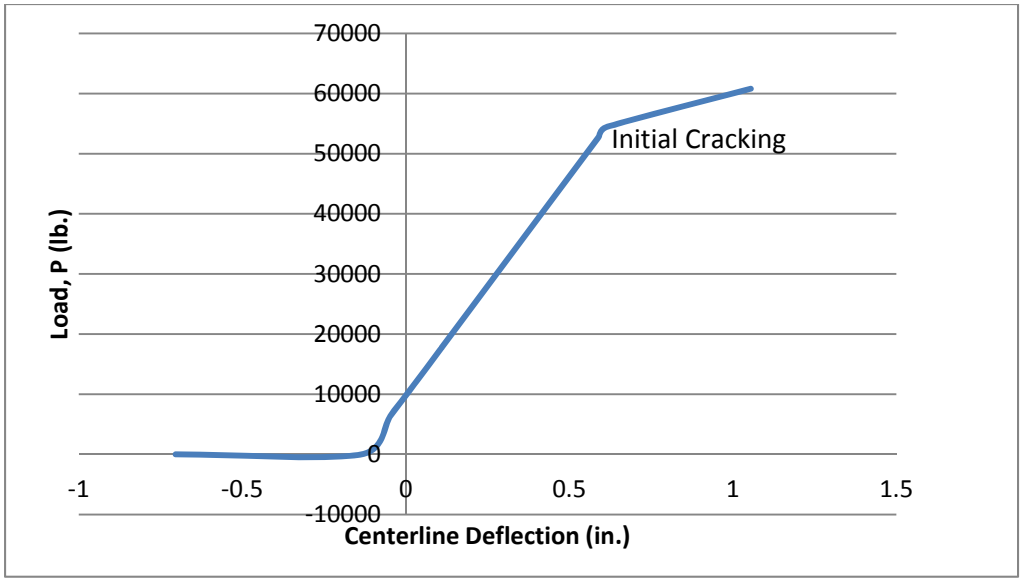

Figure 4-1 Load vs. Deflection Curve for Prestressed Concrete I-Girder

Table 4-1 Analytical Results

	ANSYS	Hand Calculations
Zero Deflection Load (lb.)	10,000	11,581
Decompression Load (lb.)	25,600	26,340
Initial Cracking Load (lb.)	54,400	54,188
Failure load (lb.)	225,552	201,806

The ANSYS program records concrete cracks and crushing at each applied load step. A circle outline in the plane of the crack represents cracking. An octahedron outline represents crushing. If a crack has opened and then closed, the circle outline will have an X through it. Each integration point can crack in up to three different planes.

The first, second, and third crack at an integration point is shown with a red circle outline, green circle outline, and blue circle outline, respectively (ANSYS, 2012). It should be noted that even micro cracks and crushing are displayed and that it is not necessarily a progression of flexural or shear cracks.

Localized cracking occurs in the concrete when prestressing is applied. When a traditional level of prestress (f_{pe}=150 ksi) was applied, these cracking was so extensive that a converged solution was not possible to obtain. For this reason the effective prestressing that was applied to the girder was 100 ksi. Figure 4-2 shows the concrete cracking at the two ends of the girder due to the application of prestress.

Figure 4-2 Localized Cracking from Effective Prestress Application

Initial cracking is defined to be the loading at which the extreme tension fiber reaches the modulus of rupture (Wolanski, 2004). Initial cracking of the beam in the ANSYS model occurs at load 54400 lbs. The hand-calculated initial cracking load is 54188 lbs. (Table 4.1 and Appendix C). Initial cracks occurred in the mid-span region and were flexural cracks. Figure 4-3 shows the initial cracking of the concrete due to applied load.

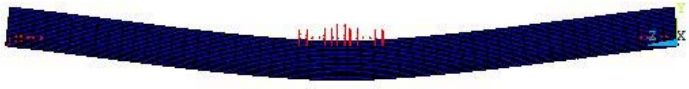

Figure 4-3 Initial Cracking

Yielding of the prestress steel is found $0.9f_{pu}$ for this model. Yielding occurred when stress of the prestressing steel was 245 ksi and applied load was 175000 lbs. Figure 4-4 shows the concrete crack pattern at yield load.

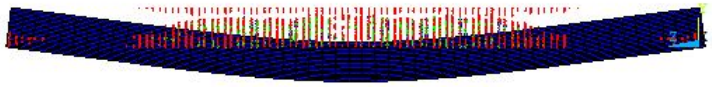

Figure 4-4 Cracking at Yield Load

At a load of 225,552 lbs. unresolvable non-convergence of the nonlinear algorithm occurred, indicating the failure load for the girder. The excessive cracking that occurred throughout the entire moment region at a load of 225,520 lbs. is shown in Figure 4-5.

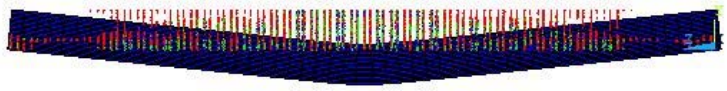

Figure 4-5 Cracking at Flexural Capacity

The progression of cracks and crushing shows an increase in the amount of flexural cracks, which indicates the flexural failure of the girder. Figure 4-6 shows the progression of cracks and crushing as the load was increased.

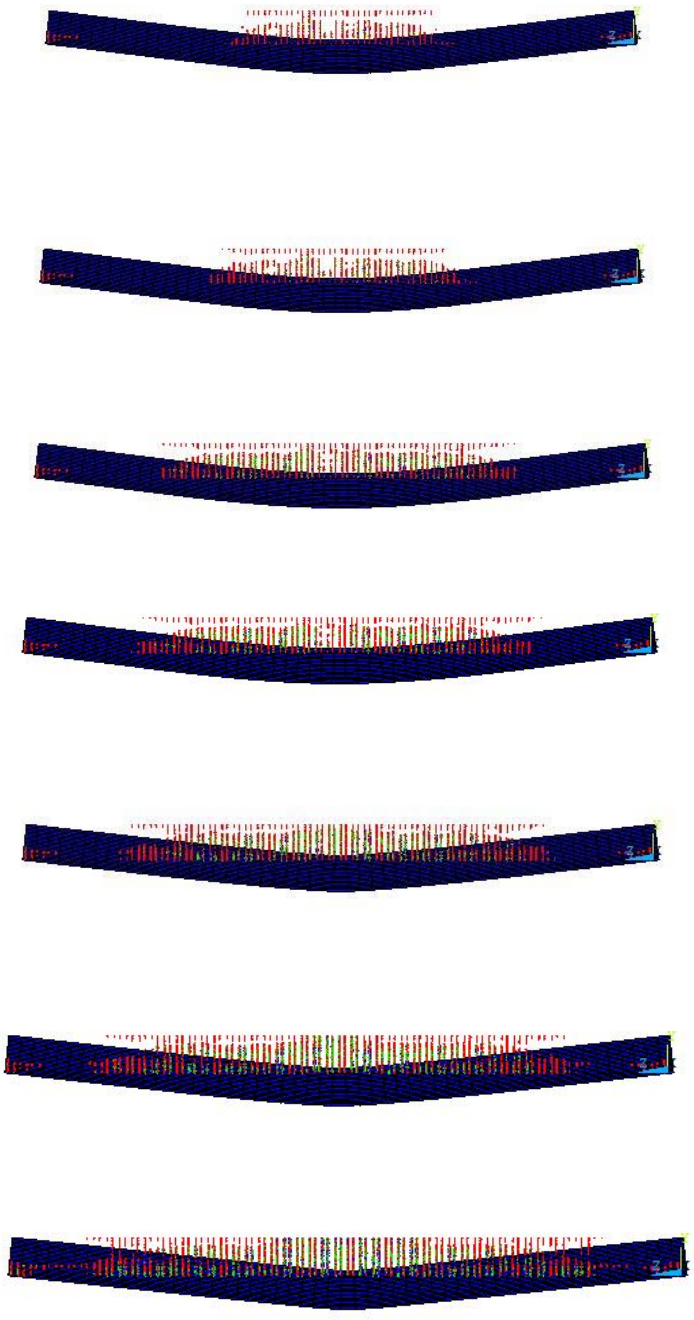

Figure 4-6 Progression of Cracks with Load Increment for Prestressed Concrete I-Girder

Hand calculations (Appendix C) predicted that the flexural capacity of the girder would correspond to 201,806 lbs. (Table 4-1) and shear capacity 198,820 lbs. The ANSYS model prediction (225,520 lbs.) corresponds very well with the hand calculations. The stress in the prestressing steel at failure predicted by ANSYS was 264,820 psi (Table 4-11). Using strain compatibility method the stress in the prestressing steel at failure was 254,485 psi (Appendix C), which corresponds well to ANSYS prediction. The strain distribution of the concrete at the flexural capacity of the girder is shown in Figure 4-7.

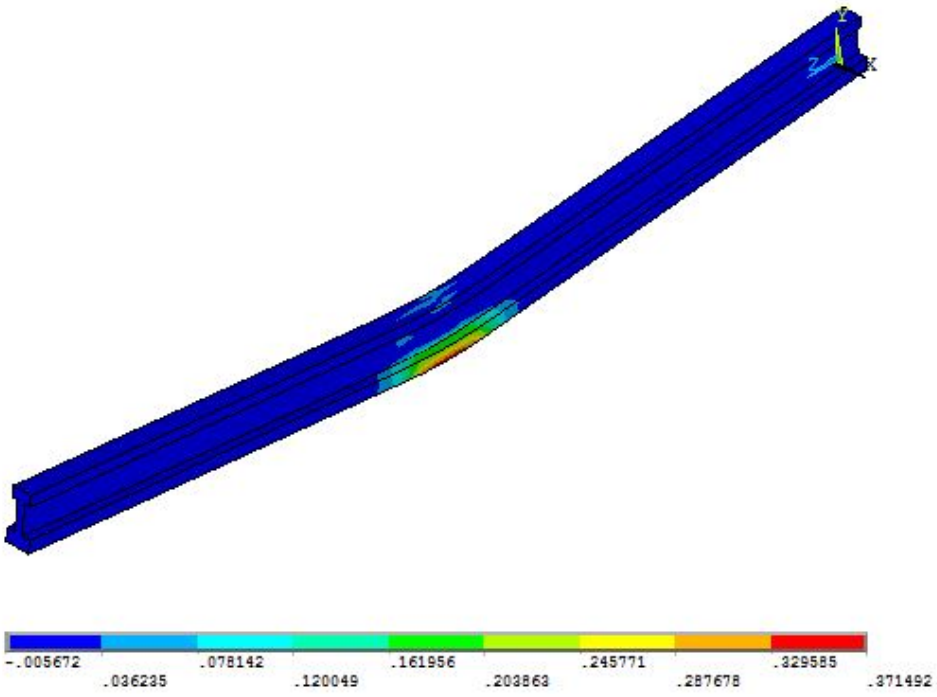

Figure 4-7 Concrete Strain at Flexural Capacity

4.2.2 Flexural Strengthening

For the flexural strengthening one layer of FRP was applied at the bottom of the girder over the entire length. The same analysis procedure as the un-strengthened girder

was followed for the strengthened girder. A listing of the load steps, sub steps, and loads applied per restart file are shown in Table A-2 in Appendix A.

The analysis results showed that the load-deflection curve for the strengthened girder had five distinct points due to the application of prestress and load increments. As seen in Figure 4-8, these distinct points are effective prestress, addition of self-weight, initial cracking, steel yielding, and failure.

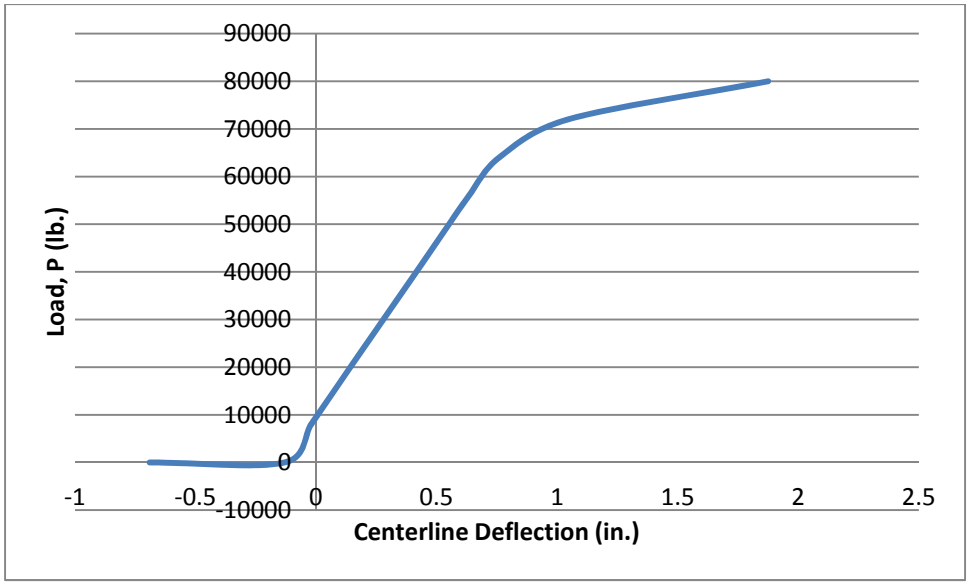

Figure 4-8 Load vs. Deflection Curve for Prestressed Concrete I-Girder Strengthened for Flexure

There was 17.65%, 5.14%, and 13.52% increase due to flexural strengthening as compared to the un-strengthened girder for the cracking load, yielding load, and ultimate load respectively. The deflection at the ultimate load decreased 35% due to flexural strengthening. The summary of the ANSYS results can be seen in Table 4-2.

Table 4-2 Summary of ANSYS Results

Load Levels	Un-strengthened Girder	Strengthened Girder	% Increase
Cracking Load (lb.)	54400	64000	17.65
Yielding Load (lb.)	175000	184000	5.14
Ultimate Load (lb.)	225520	256000	13.52
Deflection at Cracking Load(in.)	0.612	0.76	24.2

Localized cracking at the two ends of the girder that occurs due to the application of prestress was reduced by the FRP strengthening of the girder. The concrete crack plot due to prestressing and self-weight is shown in Figure 4-9.

Figure 4-9 Localized Cracking from Effective Prestress Application and Self Weight

The initial cracking load for FRP strengthened girder agaist flexure was 64000 lb. (Table 4-2). Initial cracks occurred in the mid span region with reduced flexural cracks in height as compared to unstrengthened girder. The concrete crack plot due to initial cracking load is shown in Figure 4-10.

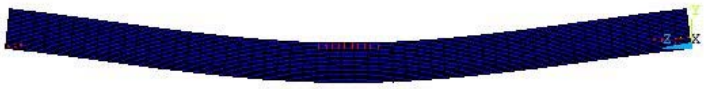

Figure 4-10 Initial Cracking

Yielding of the prestress steel is found $0.95f_{pu}$ for the FRP strengthened girder against flexure. Yielding occurred when stress of the prestressing steel was 257 ksi and applied load was 184 kips. Figure 4-11 shows the concrete crack pattern for the FRP strengthened girder at yield load.

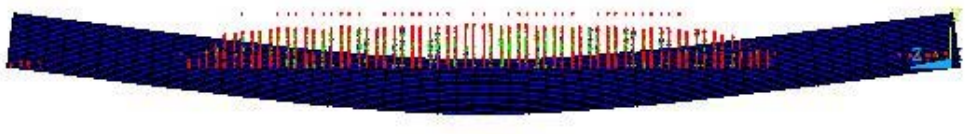

Figure 4-11 Cracking at Yield Load

At a load of 256 kips unresolvable non-convergence of the nonlinear algorithm occurred, indicating the failure load for the girder. The excessive cracking that occurred throughout the entire span length at a load of 256 kips is shown in Figure 4-12.

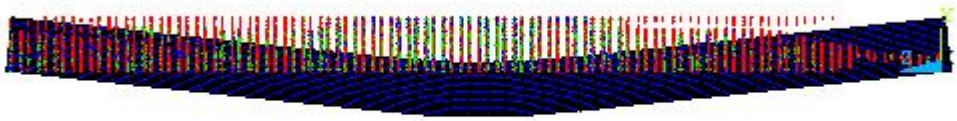

Figure 4-12 Cracking at Flexural Capacity

The crack progression for the FRP strengthened girder showed a reduction in the height of the flexural cracks and the area of concrete subjected to flexural cracks as compared to unstrengthened girder. Figure 4-13 shows the progression of cracks with the load increment for the prestressed girder strengthened against flexure.

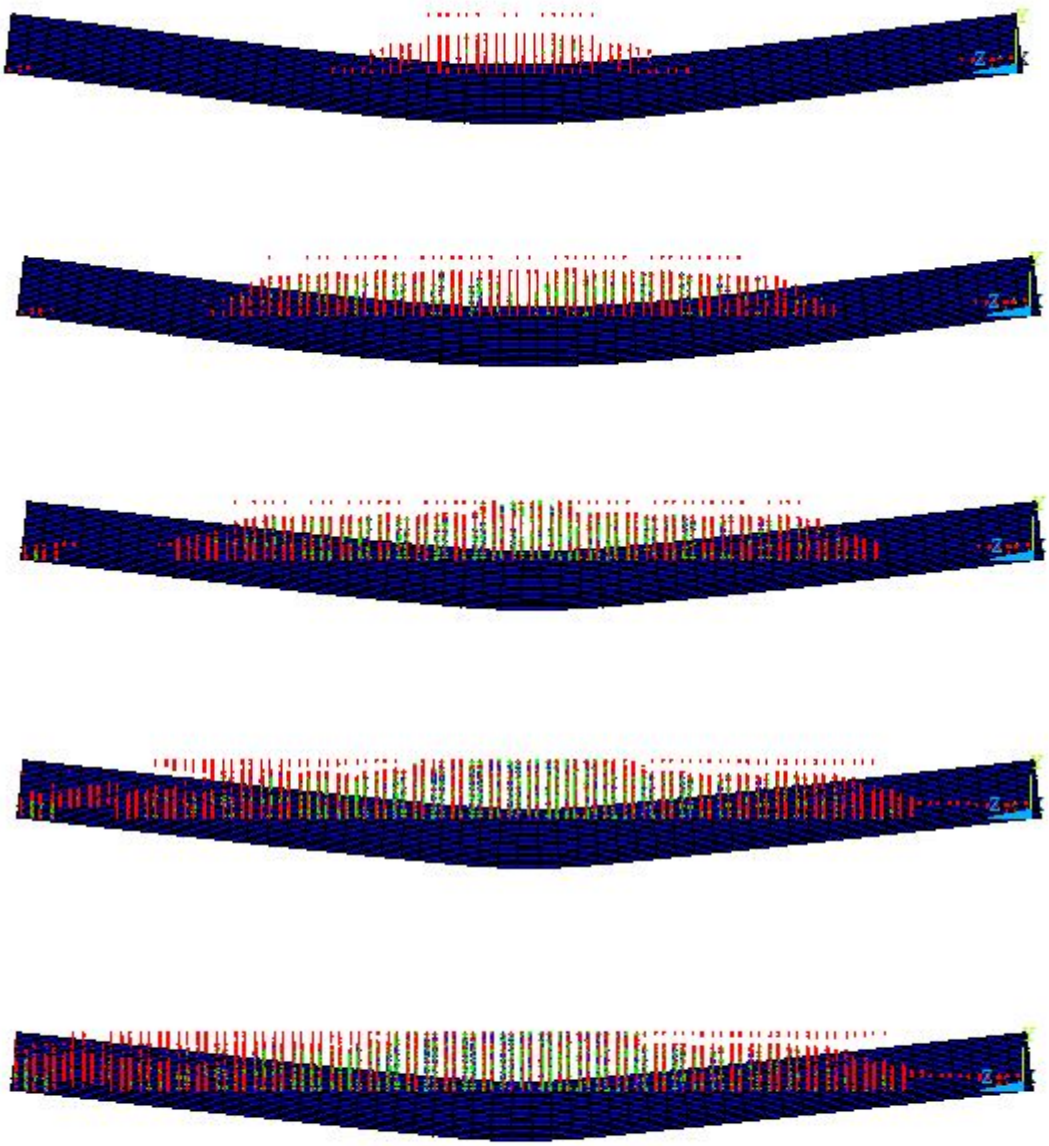

Figure 4-13 Progression of Cracks with Load Increment for Prestressed Concrete I-Girder Strengthened for Flexure

The nominal moment capacity of the modeled FRP strengthened girder was calculated following the steps reported in ACI 440-2R. The step by step calculations are

shown in Appendix C. Hand calculations (Appendix C) predicted that the flexural capacity of the girder would correspond to 213,230 lbs. (Table 4-3). The ANSYS model prediction (256,000 lbs.) corresponds very well with the hand calculations. The stress in the prestressing steel at failure predicted by ANSYS was 264,820 psi (Table 4-9). Using strain compatibility method the stress in the prestressing steel at failure was 252,670 psi (Appendix C), which also corresponds well to ANSYS prediction.

The FRP stress distribution at the flexural capacity of the girder is shown in Figure 4-14. The maximum stress in the FRP is found to be 77.284 ksi in the ANSYS model (Figure 4-14). The effective stress in the FRP is 79.074 ksi when calculated according to ACI 440-2R (Appendix C). The ultimate tensile strength of the FRP used in this model is 135 ksi which indicates that FRP rupture is not the failure mode of the girder. Hand calculation (Appendix C, Flexural Strengthening, and Step 6) and ANSYS model both agree that the failure mode of the girder is yielding of the prestressed steel followed by the concrete crushing.

According to Bakis et al. (2002), sections with smaller amounts of FRP reinforcement fail by FRP tensile rupture, while larger amounts of FRP reinforcement result in failure by crushing of the concrete prior to the attainment of ultimate tensile strain in the outermost layer of FRP reinforcement. They mentioned that underreinforced flexural sections experience a sudden tensile rupture instead of a gradual yielding because of the elasticity in FRP materials. They concluded that the concrete crushing failure mode of an overreinforced member is somewhat more desirable, which leads to a more gradual failure mode by enhanced energy absorption and greater deformability.

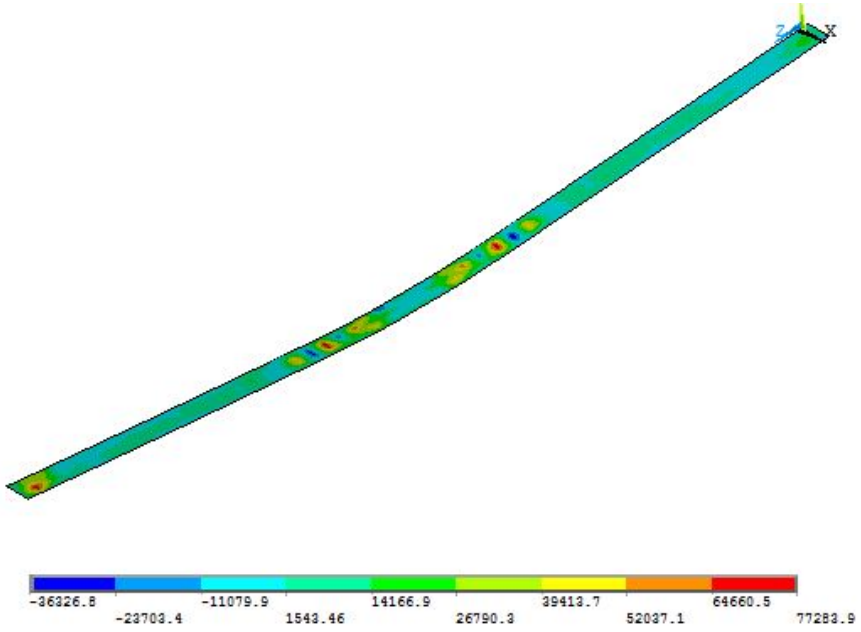

Figure 4-14 FRP Stress at Flexural Capacity

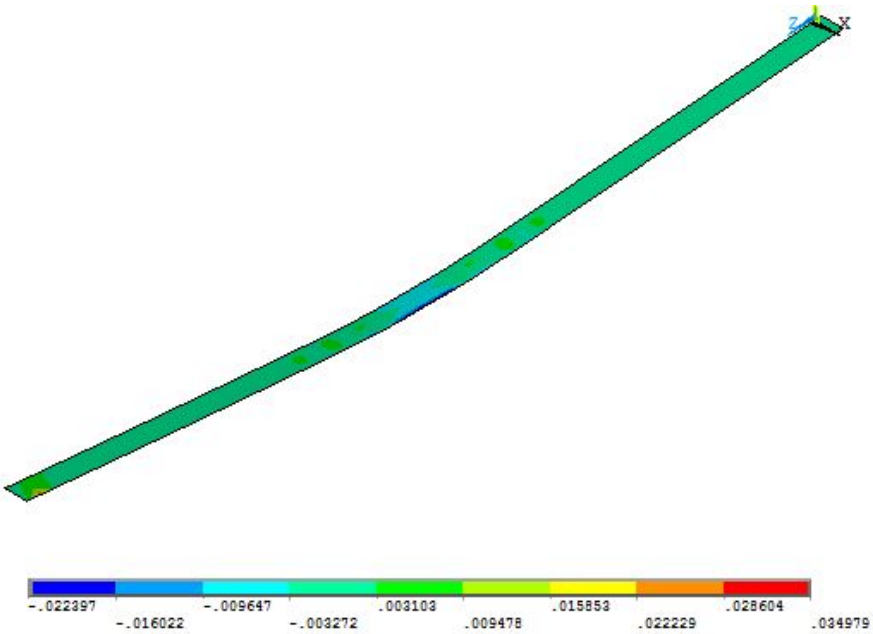

Figure 4-15 FRP Strain at Flexural Capacity

The strain distribution of the FRP at the flexural capacity is shown in Figure 4-15. The figure shows that the strain of the FRP is well below the rupture strain 0.015 in/in. The hand calculated effective strain of FRP is 0.008786 in/in (Appendix C), which indicates good prediction of the ANSYS model. The strain distribution of the concrete at the flexural capacity of the girder is shown in Figure 4-16.

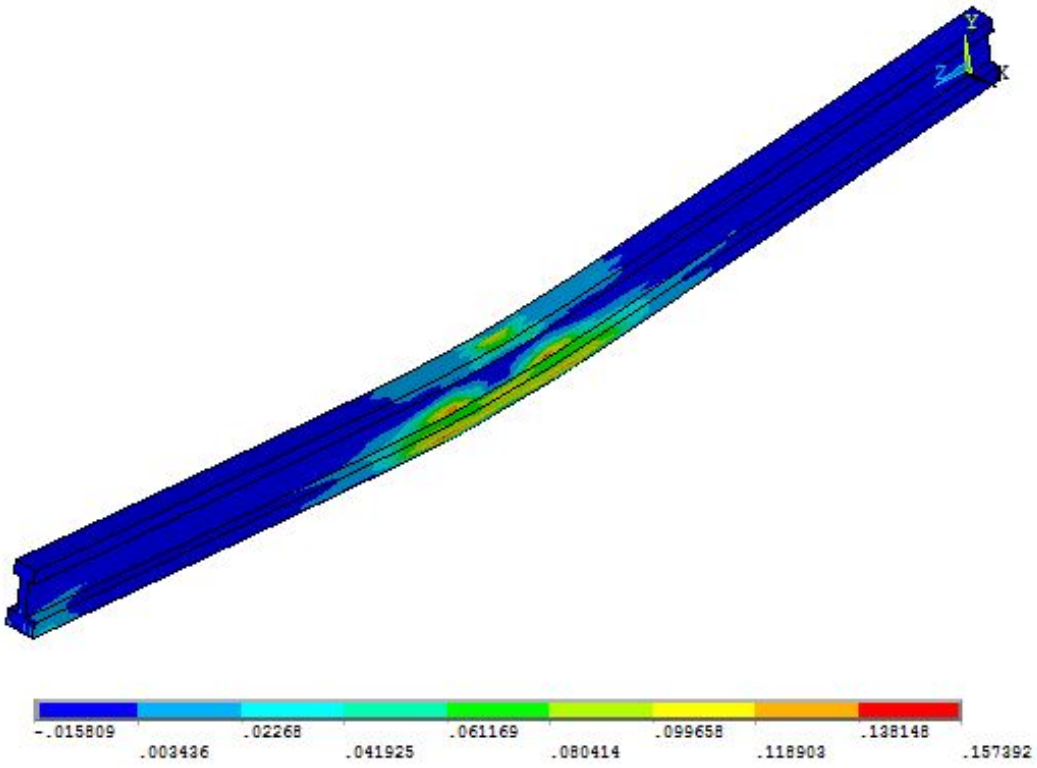

Figure 4-16 Concrete Strain at Flexural Capacity

The percentage of the increased load capacity due to flexural strengthening was 5.66% according to ACI 440-2R. Table 4-3 shows the comparison of hand calculation and ANSYS results.

Table 4-3 Comparison of Hand Calculation and ANSYS Results

	Un-strengthened Girder	Strengthened Girder	% Increase	Failure Mode
Nominal Strength by Hand Calculation (kip)	202	213.23	5.66	Yielding of steel followed by concrete crushing
Ultimate Load from ANSYS (kip)	225.52	256	13.52	Yielding of steel followed by concrete crushing

4.2.3 Shear Strengthening

For the shear strengthening one layer of FRP was applied as U-wrap over the entire length. Two types of strengthening configuration were used – vertical and 45 degree inclined. The same analysis procedure as the un-strengthened girder was followed for the shear-strengthened girder. A listing of the load steps, sub steps, and loads applied per restart file are shown in Table A-3 in Appendix A.

The analysis results showed that the load-deflection curve for the shear-strengthened girder had five distinct points due to the application of prestress and load increments. Figure 4-17 shows the load-deflection curve for the vertical U-wrap shear strengthened prestressed concrete girder. As seen in Figure 4-17, these distinct points are effective prestress, addition of self-weight, initial cracking, steel yielding, and failure.

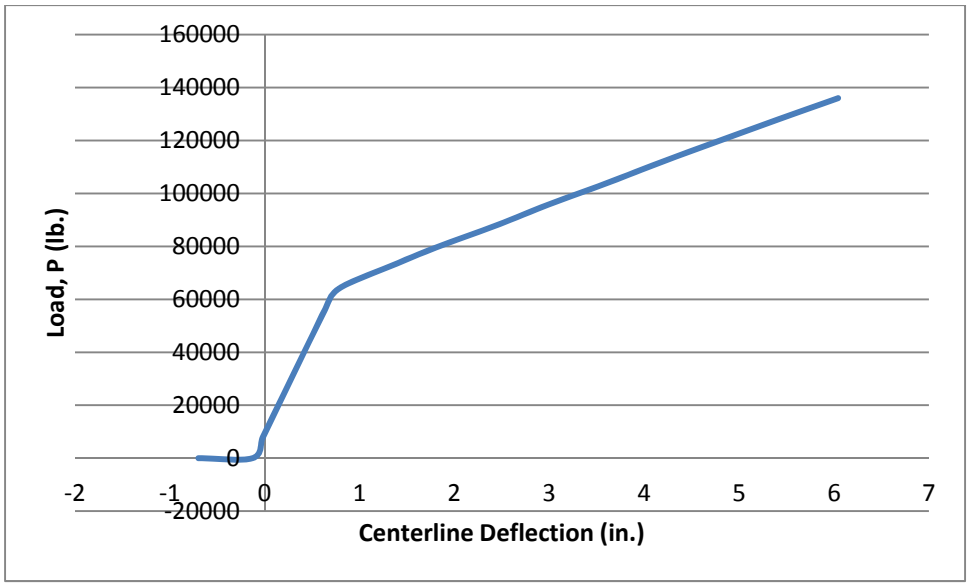

Figure 4-17 Load vs. Deflection Curve for Prestressed Concrete I-Girder Strengthened for Shear

There was 17.65%, 18.86%, and 112% increase due to vertical U-wrap shear strengthening as compared to the un-strengthened girder for the cracking load, yielding load, and ultimate load respectively. The deflection at the ultimate load increased 88.8% due to shear strengthening. The summary of the ANSYS results can be seen in Table 4-4.

Table 4-4 Summary of ANSYS Results

Load Levels	Un-strengthened Girder	Strengthened Girder	% Increase
Cracking Load (lb.)	54400	64000	17.65
Yielding Load (lb.)	175000	208000	18.86
Ultimate Load (lb.)	225520	480000	112
Deflection at Cracking Load(in.)	0.612	0.7804	27.52

Localized cracking at the two ends of the girder that occurs due to the application of prestress are shown in Figure 4-18.

Figure 4-18 Localized Cracking from Effective Prestress Application

The initial cracking load for FRP strengthened girder agaist shear was 64000 lb. (Table 4-4). Initial cracks occurred in the mid span region with reduced flexural cracks in height as compared to unstrengthened girder. The concrete crack plot due to initial cracking load is shown in Figure 4-19.

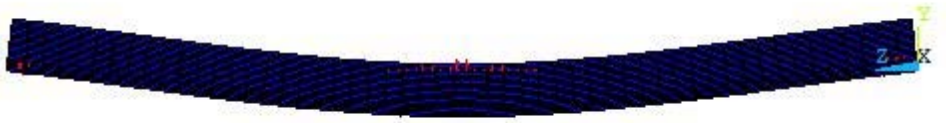

Figure 4-19 Initial Cracking

Yielding of the prestress steel is found $0.95f_{pu}$ for the FRP strengthened girder against shear. Yielding occurred when stress of the prestressing steel was 257.18 ksi and applied load was 208000 lbs. Figure 4-20 shows the concrete crack pattern for the FRP strengthened girder at yield load.

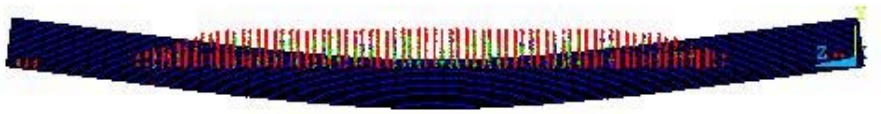

Figure 4-20 Cracking at Yield Load

At a load of 496,000 lbs. unresolvable non-convergence of the nonlinear algorithm occurred, indicating the failure load for the girder. The excessive cracking that occurred throughout the entire span length at a load of 480,000 lbs. is shown in Figure 4-21.

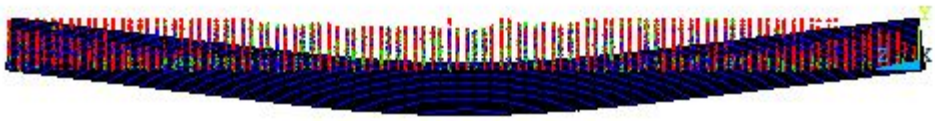

Figure 4-21 Cracking at Ultimate Capacity

The crack progression for the FRP strengthened girder showed a reduction in the height of the shear cracks and the area of concrete subjected to shear cracks as compared to unstrengthened girder. Figure 4-22 shows the progression of cracks with the load increment for the prestressed girder strengthened against shear.

Figure 4-22 Progression of Cracks with Load Increment for Prestressed Concrete I-Girder Strengthened for Shear

The shear capacity of the modeled FRP strengthened girder was calculated following the steps reported in ACI 440-2R. The step by step calculations are shown in Appendix C. Hand calculations (Appendix C) predicted that the load capacity of the shear strengthened girder would correspond to 403,500 lbs. (Table 4-5). The ANSYS model prediction (480,000 lbs.) corresponds well with the hand calculations. The stress in the prestressing steel at failure predicted by ANSYS was 264,820 psi (Table 4-9).

The FRP stress distribution at the ultimate capacity of the girder is shown in Figure 4-23. The maximum stress in the FRP is found to be 99.402 ksi in the ANSYS model (Figure 4-23). The effective stress in the FRP is 36 ksi when calculated according to ACI 440-2R (Appendix C, Shear Strengthening, and Step 3). The ultimate tensile strength of the FRP used in this model is 135 ksi which indicates that FRP rupture does not limit the shear capacity of the girder. The failure mode of the girder is yielding of the prestressed steel followed by the concrete crushing.

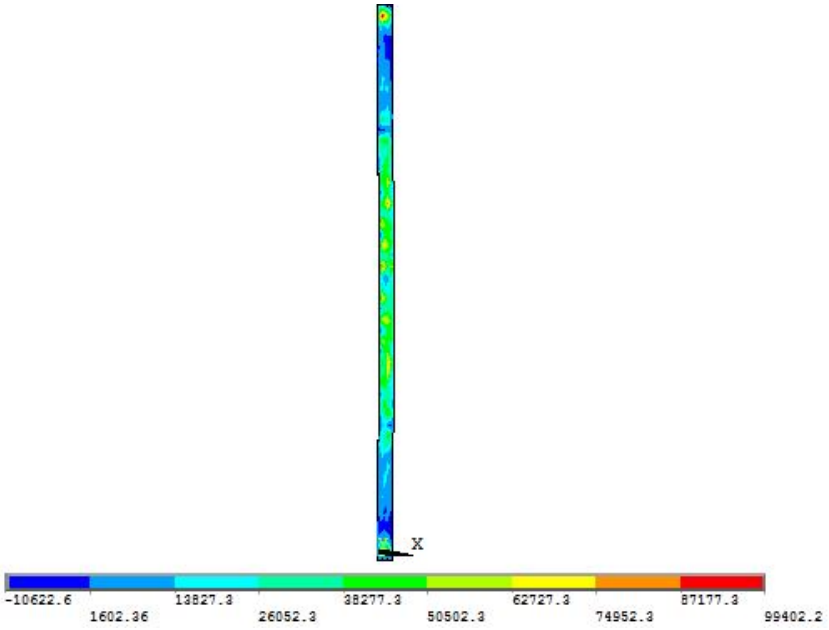

Figure 4-23 FRP Stress Distribution at Ultimate Capacity (Bottom View)

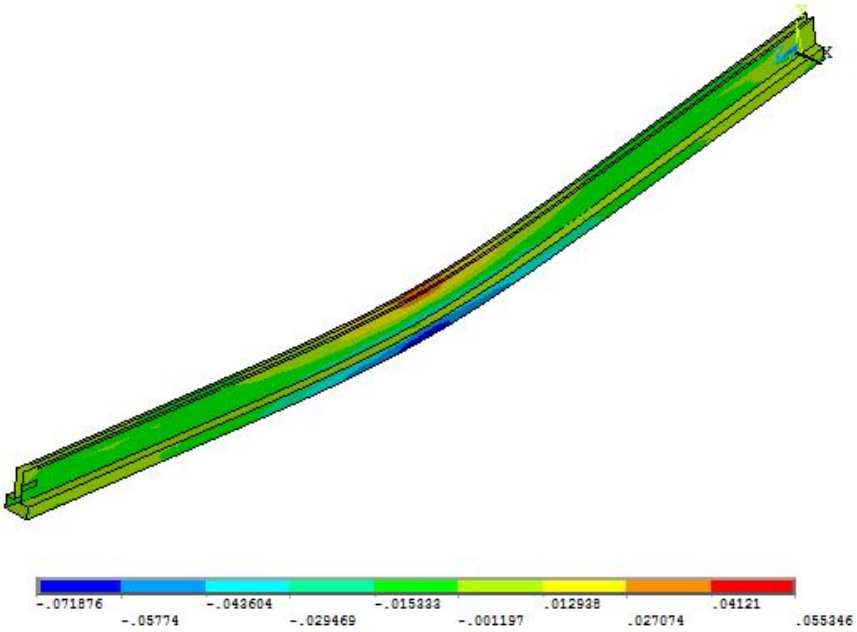

Figure 4-24 FRP Strain Distribution at Ultimate Capacity

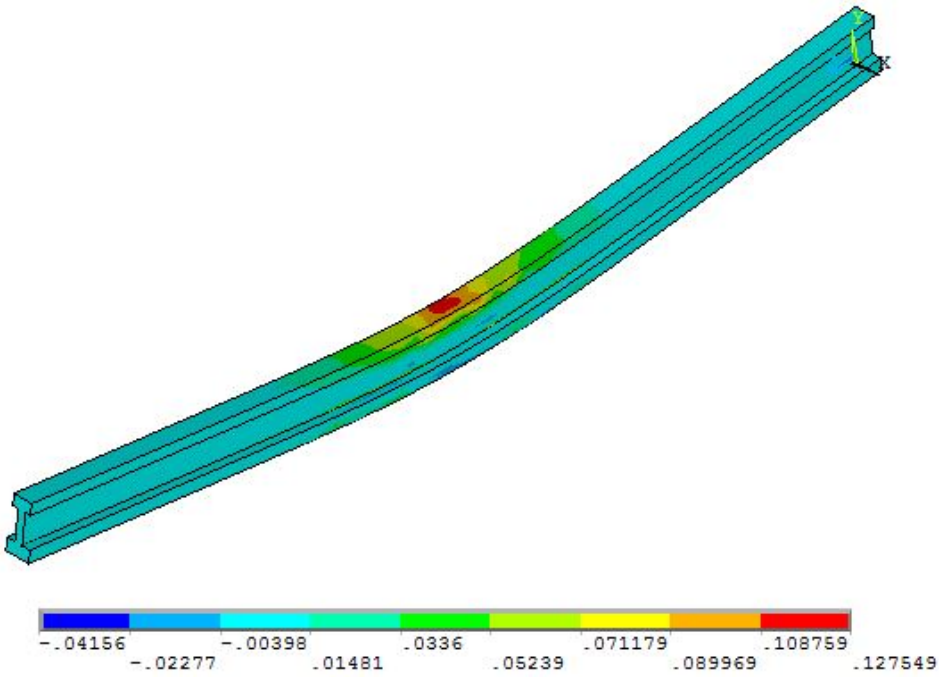

Figure 4-25 Concrete Strain at Ultimate Capacity

The strain distribution of the FRP at the ultimate capacity is shown in Figure 4-24. The figure shows that the strain of the FRP has reached near the rupture strain 0.015 in/in in both sides of the girder. The strain distribution of the concrete at the ultimate capacity of the girder is shown in Figure 4-25.

The percentage of the increased load capacity due to shear strengthening was 85.54% according to ACI 440-2R. Table 4-5 shows the comparison of hand calculation and ANSYS result.

Table 4-5 Comparison of Hand Calculation and ANSYS Results

	Un-strengthened Girder	Strengthened Girder	% Increase
Load Capacity by Hand Calculation (kip)	217.47	403.5	85.54
Ultimate Load from ANSYS (kip)	225.52	480	112

The influence of fiber orientation on the ultimate strength of the prestressed concrete girder strengthened for shear was investigated. For this reason, the orientation angle of the FRP was changed to 45 degree and nonlinear analysis for the girder was performed. The analysis results are shown in Table A-4 in Appendix A. The ultimate load capacity of the girder was increased due to the inclination of the FRP. The load-deflection curve for the inclined FRP strengthened girder is shown in Figure 4-26. The percentage of the increased load capacity due to shear strengthening at 45 degree angle was 121 according to ACI 440-2R (Appendix C). Table 4-6 shows the comparison of hand calculation and ANSYS results.

Table 4-6 Comparison of Hand Calculation and ANSYS Results

	Un-strengthened Girder	Strengthened Girder	% Increase
Load Capacity by Hand Calculation (kip)	217.47	480.6	121
Ultimate Load from ANSYS (kip)	225.52	544	141.2

Figure 4-26 combines the load-deflection curves for un-strengthened girder, FRP strengthened girder for flexure, vertical U-wrap strengthened girder for shear, and 45 degree inclined U-wrap strengthened girder.

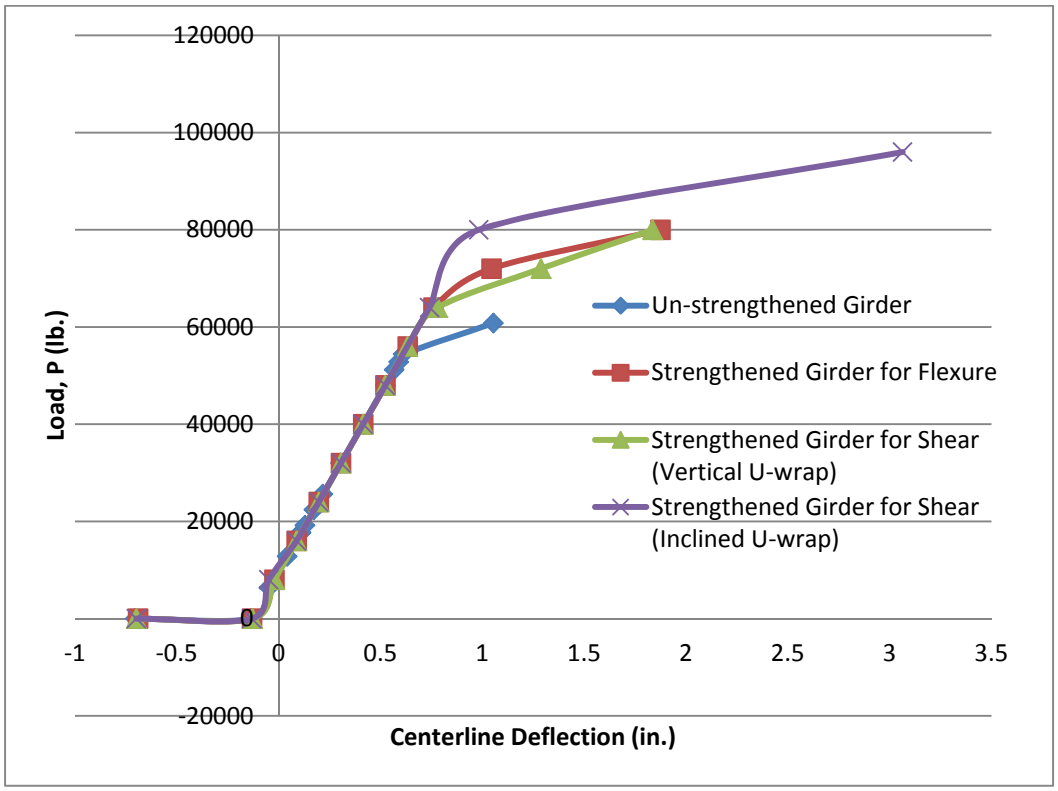

Figure 4-26 Load vs. Deflection Curve for Prestressed Concrete I-Girder Strengthened for Flexure and Shear

The stress and strain values of the pre-stressing steel and FRP at the initial cracking for the un-strengthened and FRP strengthened girder are shown in Table 4-7.

Table 4-7 Comparison at Initial Cracking

	Un-strengthened Girder	Strengthened Girder for Flexure	Strengthened Girder for Shear
Load (lb.)	54400	64000	64000
Pre-stressing Steel Stress (ksi)	101.91	103.85	105.83
Pre-stressing Steel Strain	0.0036398	0.0037090	0.0037798
Maximum Stress of FRP (psi)		12712.8	12652.9
Maximum Strain of FRP		0.001411	0.001405

The stress and strain values of the pre-stressing steel and FRP at yielding for the un-strengthened and FRP strengthened girder are shown in Table 4-8. As seen in the table, 9.4% of the ultimate tensile strength of the FRP was used in case of flexural strengthening while 13.2% was used in case of shear strengthening (U-wrap).

Table 4-8 Comparison at Yielding

	Un-strengthened Girder	Strengthened Girder for Flexure	Strengthened Girder for Shear
Load (lb.)	175000	184000	208000
Pre-stressing Steel Stress (ksi)	245.4	257.57	257.18
Pre-stressing Steel Strain	0.010599	0.013898	0.013563
Maximum Stress of FRP (psi)		12709.3	17758.1
Maximum Strain of FRP		0.001411	0.004844

The stress and strain values of the pre-stressing steel and FRP at ultimate capacity for the un-strengthened and FRP strengthened girder are shown in Table 4-9. As seen in the table, 57% of the ultimate tensile strength of the FRP was used in case of flexural strengthening while 74% was used in case of shear strengthening (U-wrap).

Table 4-9 Comparison at Ultimate Capacity

	Un-strengthened Girder	Strengthened Girder for Flexure	Strengthened Girder for Shear
Load (lb.)	225520	256000	480000
Pre-stressing Steel Stress (ksi)	264.82	264.82	264.82
Pre-stressing Steel Strain	0.59936	0.23635	0.20351
Maximum Stress of FRP (psi)		77284	99402
Maximum Strain of FRP		0.0349	0.0553

FRP application reduced concrete cracking and deflection of the girder. Figure 4-27 shows how concrete crack pattern and deflection varied due to FRP strengthening for flexure and shear when 160 kip load was applied.

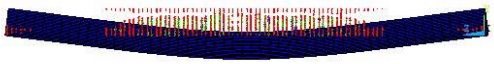

Un-strengthened Girder

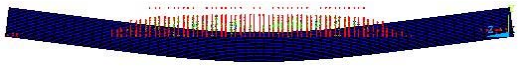

Strengthened Girder for Flexure

Strengthened Girder for Shear

Figure 4-27 Crack Pattern under 160 kip Load

Figure 4-28 shows how concrete crack pattern and deflection varied due to FRP strengthening for flexure and shear when 192 kip load was applied. The mid span deflection was 47% decreased in case of flexural strengthening and 61% decreased in case of vertical U-wraps compared to un-strengthened girder. Also, the height of the concrete cracks was significantly reduced in case of FRP strengthening.

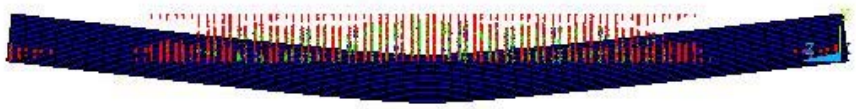

Un-strengthened Girder

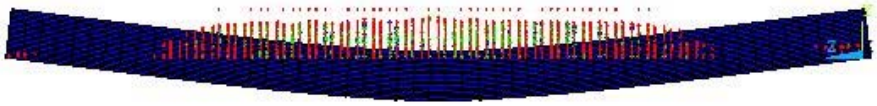

Strengthened Girder for Flexure

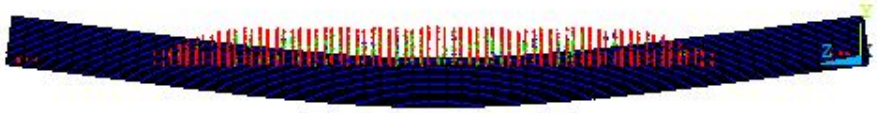

Strengthened Girder for Shear

Figure 4-28 Crack Pattern under 192 kip Load

Figure 4-29 shows how concrete crack pattern varied due to FRP strengthening for flexure and shear when 216 kip load was applied.

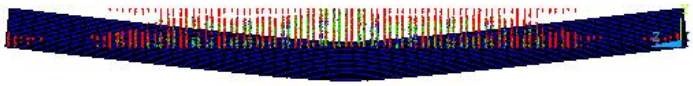

Un-strengthened Girder

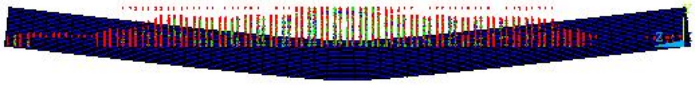

Strengthened Girder for Flexure

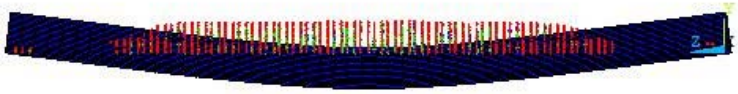

Strengthened Girder for Shear

Figure 4-29 Crack Pattern under 216 kip Load

Figure 4-30 shows how concrete crack pattern varied due to FRP strengthening for flexure and shear when 232 kip load was applied.

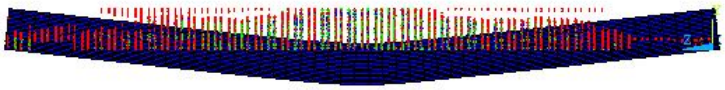

Strengthened Girder for Flexure

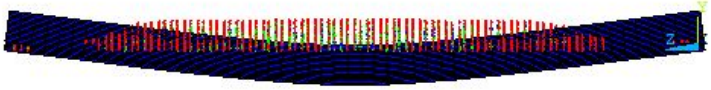

Strengthened Girder for Shear

Figure 4-30 Crack Pattern under 232 kip Load

The FRP effectively increased the load carrying capacity of the girder, reduced flexural and shear crack, and reduced deflection of the girder though ductility was reduced due to strengthening. The strain in the prestressing steel at the nominal strength should be checked to maintain a sufficient degree of ductility (ACI 440, 2008). According to ACI 440, adequate ductility is achieved if the strain in the prestressing steel at the nominal strength is at least 0.013. In this study, the strain in the prestressing steel at the nominal strength was 0.011 for flexural strengthening. To account for this less ductile failure, the strength reduction factor has to be decreased. According to Equation 2.4, the strength reduction factor will be 0.77. To increase the ductility of the strengthened member, the area of the prestressing steel and the FRP should be less than that is used in this particular girder. Also, the strength of the FRP was not completely used in the ultimate capacity of the FRP strengthened girder. The use of optimum amount of prestressing steel and FRP can be result in the adequate ductility and complete use of the FRP strength for the FRP strengthened prestressed girder.

Chapter 5

Conclusion

5.1 Findings

In this thesis, an AASHTO-type IV prestressed concrete girder was modeled using ANSYS 14.5 that was eventually strengthened with FRP for flexure and shear. Flexural and shear failure were studied for un-strengthened and strengthened girder, which was compared with theoretical values obtained via accepted methods of hand calculation. The following conclusions can be made based on the evaluation of the analysis of the un-strengthened and FRP strengthened prestressed concrete AASHTO girder.

- AASHTO-type IV prestressed concrete girder was successfully modeled using finite element software ANSYS in a simpler, cheaper, and effective way compared with full scale experimental tests.
- For the un-strengthened girder, camber due to the initial prestress force and after application of the self-weight of the girder compares well to analytical values. Zero deflection, decompression, initial cracking, and failure loads were close to analytical results.
- For the flexural strengthening, good prediction was made by ANSYS in terms of flexural capacity, stress in the prestressed steel, effective stress in the FRP, and strain distribution of the FRP at ultimate capacity when compared to ACI 440.
- Results from ANSYS showed 13.52% increase in flexural capacity in case of flexural strengthening with FRP compared to un-strengthened girder. On the other hand, 5.66% increase in flexural capacity was found

according to ACI 440. This indicates that ACI 440 is conservative in predicting the flexural capacity of a FRP strengthened AASHTO girder.

- ACI 440 and ANSYS simulation both found that the failure mode of the FRP strengthened girder against flexure was yielding of the prestressed steel followed by concrete crushing, which proves that ANSYS 14.5 is capable of predicting crack patterns and failure modes of the FRP strengthened girders. Failure by concrete crushing is desired due to greater deformability that leads to a more gradual mode of failure (Bakis et al., 2002).
- In case of shear strengthening, the maximum stress in FRP at the ultimate capacity was found to be 99 ksi using ANSYS model while effective stress in the FRP according to ACI 440 was 36 ksi. ACI 440 provided guidance on determining effective strain of FRP for shear strengthening of reinforced concrete members. This effective strain of FRP differed for shear strengthening of prestressed concrete girder.
- In case of shear strengthening using vertical U-wraps, 112% increase in ultimate load capacity was found through ANSYS compared to un-strengthened girder while according to ACI 440 this increase 85.54%.
- For shear strengthening 141% increase in load capacity was observed by using ANSYS model compared to the un-strengthened girder when FRP U-wraps were inclined at 45 degree angle. According to ACI 440, 121% increase in load capacity was calculated.
- The addition of FRP to the prestressed concrete girder showed a decrease in amount of deflection at various loads. For example, when 192 kips load was applied at the mid span of the girder, the mid span

deflection was 47% decreased in case of flexural strengthening and 61% decreased in case of vertical U-wraps compared to un-strengthened girder.

- The results obtained from the finite element analysis demonstrate that FRP can be used as an effective strengthening technique.

5.2 Limitations

The following are identified as the limitations of this research:

- Material nonlinearity had not been taken into account in case of FRP modeling.
- Epoxy between the concrete and FRP was modeled without considering debonding criteria.
- Applied effective prestress force was 37 percent of the tensile strength of flexural reinforcement, which is less than the practical use.
- Experimental evaluation had not been performed.
- This study focused on flexure and shear strength of the girder, long term effects and effects of impact loading had not been taken into account.

5.3 Recommendations for Future Study

The literature review and analysis procedure utilized in this thesis has provided useful insight for future application of a finite element package as a method of analysis for FRP strengthened prestressed concrete AASHTO-type girders. Based on the results of this research, the following future research is recommended:

- While modeling the prestressed beam, relaxation losses due to prestress, creep, shrinkage, and elastic shortening were lumped together in a single load step. Individual modeling of those losses could be included in future research.

- More full scale experimental tests need to be conducted, which will allow more researches to use their results to validate finite element model.
- The finite element results are compared with ACI 440 in this present study. In future, other codes could be compared with.
- Simulation of debonding phenomenon is candidate for future research.
- In this study, only point load at the mid span of a simply supported girder was considered. Other load and boundary conditions should be analyzed for future study.
- Effect of FRP strengthening on axially loaded column could be studied in future.

Appendix A

Finite Element Analysis Results

Table A-1 Load Increments for the Analysis of the Prestressed Concrete Girder

Beginning Time	Time at End of Load step	Load Step	Sub Step	Load Increment (lb.)	Deflection (in)
0	55000	1	2	Prestress	-0.7036
55000	56000	2	2	Self weight	-0.1357
56000	57000	3	1	6400	-0.047
57000	58000	4	1	6400	0.042
58000	59000	5	1	4800	0.1079
59000	60000	6	1	80	0.1089
60000	61000	7	1	16	0.1092
61000	62000	8	1	16	0.1094
62000	63000	9	1	1488	0.1296
63000	64000	10	1	3200	0.1736
64000	65000	11	1	3200	0.2175
65000	66000	12	1	6400	0.3047
66000	67000	13	1	8000	0.4148
67000	68000	14	1	8000	0.5244
68000	69000	15	1	3200	0.5682
69000	70000	16	1	1600	0.5901
70000	71000	17	1	1600	0.612
71000	720000	18	1	6400	1.055
720000	730000	19	9	800	1.0587
730000	740000	20	201	2400	1.134
740000	750000	21	201	16000	2.2249
750000	760000	22	201	16000	3.3125
760000	770000	23	201	16000	4.6332
770000	780000	24	201	16000	6.0087
780000	790000	25	201	16000	7.438
790000	800000	26	201	16000	9.042
800000	810000	27	201	16000	11.099
810000	820000	28	201	16000	29.697
820000	830000	29	201	16000	34.6314
830000	840000	30	201	16000	41.574
840000	850000	31	201	16000	48.097
850000	860000	32	201	800	54.558
860000	870000	33	201	800	60.969
870000	880000	34	201	800	67.4616
880000	890000	35	201	800	74.154
890000	900000	36	201	800	81.197
900000	910000	37	201	800	88.5947
910000	920000	38	201	800	96.3735
920000	930000	39	201	400	104.192
930000	940000	40	201	160	111.903
940000	950000	41	201	160	119.625
950000	960000	42	201	80	127.185
960000	970000	43	201	80	134.64
970000	980000	44	201	80	142.319
980000	990000	45	201	80	149.678
990000	1000000	46	201	80	157.195

Table A.1 - *Continued*

1000000	1100000	47	201	80	164.416
1100000	1200000	48	201	80	171.846
1200000	1300000	49	201	80	179.141
1300000	1400000	50	201	80	186.465
1400000	1500000	51	201	80	193.83
1500000	1600000	52	201	80	201.235
1600000	1700000	53	201	80	208.558
1700000	1800000	54	201	80	215.88
1800000	1900000	55	201	80	223.06
1900000	2000000	56	201	80	230.381
2000000	2100000	57	201	80	237.826
2100000	2200000	58	201	80	245.234
2200000	2300000	59	201	80	252.654
2300000	2400000	60	201	80	259.919
2400000	2500000	61	201	80	267.446
2500000	2600000	62	201	32	Failed

Table A-2 Load Increments for the Analysis of the Prestressed Concrete Girder Strengthened with Longitudinal FRP

Beginning Time	Time at End of Load step	Load Step	Sub Step	Load Increment (lb.)	Deflection (in)
0	5120	1	1	Prestress	-0.69
5120	5500	2	1	Self weight	-0.1303
55000	56000	3	4	8000	-0.0206
56000	57000	4	4	8000	0.0884
57000	58000	5	4	8000	0.1969
58000	59000	6	4	8000	0.3063
59000	60000	7	4	8000	0.4157
60000	61000	8	4	8000	0.5248
61000	62000	9	4	8000	0.6342
62000	63000	10	4	8000	0.7599
63000	64000	11	4	8000	1.0454
64000	65000	12	4	8000	1.875
65000	66000	13	4	8000	2.550
66000	67000	14	4	8000	3.039
67000	68000	15	4	8000	3.806
68000	69000	16	4	8000	4.381
69000	70000	17	4	8000	5.085
70000	71000	18	4	8000	5.6857
71000	72000	19	4	8000	6.3748
72000	73000	20	4	8000	7.11425
73000	74000	21	4	8000	7.8187
74000	75000	22	4	8000	8.57154
75000	76000	23	4	8000	9.448
76000	77000	24	4	8000	10.587
77000	78000	25	4	8000	12.325
78000	79000	26	4	8000	15.6953

Table A.2 - *Continued*

79000	80000	27	4	8000	20.8902
80000	81000	28	4	8000	30.0264
81000	82000	29	5	8000	43.7207
82000	83000	30	6	8000	61.2025
83000	84000	31	7	8000	82.4802
84000	85000	32	8	8000	104.074
85000	86000	33	9	8000	134.024
86000	87000	34	11	8000	173.646
87000	88000	35	11	16	Failed

Table A-3 Load Increments for the Analysis of the Prestressed Concrete Girder Strengthened with Vertical U-Wrap FRP

Beginning Time	Time at End of Load step	Load Step	Sub Step	Load Increment (lb.)	Deflection (in)
0	55000	1	5	Prestress	-0.698763
55000	56001	2	4	Self weight	-0.128577
56001	57000	3	4	8000	-0.01987
57000	58000	4	4	8000	0.089
58000	59000	5	4	8000	0.1978
59000	60000	6	4	8000	0.3065
60000	61000	7	4	8000	0.4153
61000	62000	8	4	8000	0.5242
62000	63000	9	4	8000	0.633
63000	64000	10	4	8000	0.7804
64000	65000	11	4	8000	1.288
65000	66000	12	4	8000	1.8365
66000	67000	13	4	8000	2.445
67000	68000	14	4	8000	3.005
68000	69000	15	4	8000	3.613
69000	70000	16	4	8000	4.19
70000	71000	17	4	8000	4.80
71000	72000	18	4	8000	5.413
72000	73000	19	4	8000	6.042
73000	74000	20	4	8000	6.701
74000	75000	21	4	8000	7.377
75000	76000	22	4	8000	8.0455
76000	77000	23	4	8000	8.751
77000	78000	24	4	8000	9.515
78000	79000	25	4	16000	11.53
79000	80000	26	4	16000	14.471
80000	81000	27	4	16000	18.8365
81000	82000	28	4	16000	24.82
82000	83000	29	4	16000	33.181
83000	84000	30	4	16000	43.82
84000	85000	31	4	16000	57.61
85000	86000	32	4	16000	76.4
86000	87000	33	4	16000	98.9

Table A.3 - *Continued*

87000	88000	34	4	16000	125.068
88000	89000	35	4	16000	155.13
89000	90000	36	4	16000	189.053
90000	91000	37	4	16000	226.42
91000	92000	38	4	16000	268.85
92000	93000	39	4	16000	312.107
93000	94000	40	4	16000	361.938
94000	95000	41	4	16000	411.4
95000	96000	42	5	16000	462.136
96000	97000	43	5	16000	504.971
97000	98000	44	5	16000	Failed

Table A-4 Load Increments for the Analysis of the Prestressed Concrete Girder Strengthened with 45 Degree Angled U-Wrap FRP

Beginning Time	Time at End of Load step	Load Step	Sub Step	Load Increment (lb.)	Deflection (in)
0	5120	1	2	Prestress	-0.698762
5120	5500	2	2	Self weight	-0.132425
5500	5600	3	1	8000	-0.048
5600	5700	4	1	8000	0.088
5700	5800	5	1	8000	0.197
5800	5900	6	1	8000	0.306
5900	6000	7	1	8000	0.415
6000	6100	8	1	8000	0.5241
6100	6200	9	1	16000	0.74172
6200	6300	10	1	16000	0.983
6300	6400	11	1	16000	3.064
6400	6500	12	1	16000	4.214
6500	6600	13	1	16000	5.347
6600	6700	14	1	16000	6.694
6700	6800	15	1	16000	8.071
6800	6900	16	1	16000	9.714
6900	7000	17	1	16000	11.85
7000	7100	18	1	16000	15.39
7100	7200	19	1	16000	20.666
7200	7300	20	1	16000	27.76
7300	7400	21	1	16000	36.764
7400	7500	22	1	16000	47.856
7500	7600	23	1	16000	61.97
7600	7700	24	1	16000	81.08
7700	7800	25	1	16000	103.553
7800	7900	26	1	16000	130.048
7900	8000	27	1	16000	159.308
8000	8100	28	1	16000	190.741
8100	8200	29	1	16000	226.691
8200	8300	30	1	16000	263.58
8300	8400	31	1	16000	304.814

Table A.4 - *Continued*

8400	8500	32	1	16000	346.194
8500	8600	33	1	16000	390.778
8600	8700	34	1	16000	436.704
8700	8800	35	1	16000	478.332
8800	8900	36	1	16000	537.493
8900	9000	37	1	16000	589.584
9000	9100	38	1	16000	643.433
9100	9200	39	1	16000	701.638
9200	9300	40	1	16000	Failed

Appendix B

Notations

A_c = Cross-sectional area of concrete in compression member, in.^{2} (mm^2)

A_f = Area of FRP external reinforcement, in.^{2} (mm^2)

A_{fv} = Area of FRP shear reinforcement with spacing s, in.^{2} (mm^2)

A_p = Area of prestressed reinforcement in tension zone, in.^{2} (mm^2)

A_s = Area of nonprestressed steel reinforcement, in.^{2} (mm^2)

b = Width of compression face of member, in. (mm)

b_w = Web width, in. (mm)

C_E = Environmental reduction factor

c = Distance from extreme compression fiber to the neutral axis, in. (mm)

d = Distance from extreme compression fiber to centroid of tension reinforcement, in. (mm)

d_f = Effective depth of FRP flexural reinforcement, in. (mm)

d_{fv} = Effective depth of FRP shear reinforcement, in. (mm)

d_p = Distance from extreme compression fiber to centroid of prestressed reinforcement, in. (mm)

E_c = Modulus of elasticity of concrete, psi (MPa)

E_f = Tensile modulus of elasticity of FRP, psi (MPa)

E_{ps} = Modulus of elasticity of prestressing steel, psi (MPa)

E_s = Modulus of elasticity of steel, psi (MPa)

e = Eccentricity of prestressing steel, in. (mm)

f_c' = Specified compressive strength of concrete, psi (MPa)

f_{fe} = Effective stress in the FRP; stress level attained at section failure, psi (MPa)

f_{fu} = Design ultimate tensile strength of FRP, psi (MPa)

f_{fu}^* = Ultimate tensile strength of the FRP material as reported by the manufacturer, psi (MPa)

f_{ps} = Stress in prestressed reinforcement at nominal strength, psi (MPa)

f_{pu} = Specified tensile strength of prestressing tendons, psi (MPa)

f_y = Specified yield strength of nonprestressed steel reinforcement, psi (MPa)

k_1 = Modification factor applied to k_v to account for concrete strength

k_2 = Modification factor applied to k_v to account for wrapping scheme

k_v = Bond-dependent coefficient for shear

L_e = Active bond length of FRP laminate, in. (mm)

M_n = Nominal flexural strength, in.-lb (N-mm)

n = Number of plies of FRP reinforcement

P_e = Effective force in prestressing reinforcement (after allowance for all prestress losses), lb (N)

r = Radius of gyration of a section, in. (mm)

t_f = Nominal thickness of one ply of FRP reinforcement, in. (mm)

V_c = Nominal shear strength provided by concrete with steel flexural reinforcement, lb (N)

V_f = Nominal shear strength provided by FRP stirrups, lb (N)

V_n = Nominal shear strength, lb (N)

V_s = Nominal shear strength provided by steel stirrups, lb (N)

w_f = Width of FRP reinforcing plies, in. (mm)

y_b = Distance from centroidal axis of gross section, neglecting reinforcement, to extreme bottom fiber, in. (mm)

α_1 = Multiplier on f_c' to determine intensity of an equivalent rectangular stress distribution for concrete

β_1 = Ratio of depth of equivalent rectangular stress block to depth of the neutral axis

ε_{bi} = Strain level in concrete substrate at time of FRP installation (tension is positive), in./in. (mm/mm)

ε_c = Strain level in concrete, in./in. (mm/mm)

$\in_c'$ = Maximum strain of unconfined concrete corresponding to f_c', in./in. (mm/mm); may be taken as 0.002

ε_f = Strain level in the FRP reinforcement, in./in. (mm/mm)

ε_{fd} = Debonding strain of externally bonded FRP reinforcement, in./in. (mm/mm)

ε_{fe} = Effective strain level in FRP reinforcement attained at failure, in./in. (mm/mm)

ε_{fu} = Design rupture strain of FRP reinforcement, in./in. (mm/mm)

ε_{pe} = Effective strain in prestressing steel after losses, in./in. (mm/mm)

ε_{pi} = Initial strain level in prestressed steel reinforcement, in./in. (mm/mm)

ε_{pnet} = Net strain in flexural prestressing steel at limit state after prestress force is discounted (excluding strains due to effective prestress force after losses), in./in. (mm/mm)

ε_{ps} = Strain in prestressed reinforcement at nominal strength, in./in. (mm/mm)

φ = Strength reduction factor

ψ_f = FRP strength reduction factor

= 0.85 for flexure (calibrated based on design material properties)

= 0.85 for shear (based on reliability analysis) for three-sided FRP U-wrap or two-sided strengthening schemes

= 0.95 for shear fully wrapped sections

Appendix C

Hand Calculation

C.1 Calculation to Determine the Material Properties of Concrete

C.1.1 Density of Concrete

Gravitational acceleration = 386.4 in/s^2

Unit weight of concrete = 150 pcf

Therefore,

Unit mass of concrete or Density of concrete = $\frac{150}{386.4*12^3}$ = 0.0002247

C.1.2 Stress-Strain Curve for Concrete

f'$_c$ = 7000 psi

E_c = 5072000 psi

Modulus of Rupture = 7.5*$\sqrt{}$ f'$_c$ = 627.5 psi

Point 1, f = 0.3* f'$_c$ = 2100 psi

$\varepsilon = \frac{f}{E_c}$ = 0.000414 in/in

According to MacGregor 1992,

$f = \frac{E_c * \varepsilon}{1+(\frac{\varepsilon}{\varepsilon^\circ})^2}$

$\varepsilon^\circ = \frac{2f_c'}{E_c}$

$E_c = \frac{f}{\in}$

Where,

f = stress at any strain ε, psi

ε = strain at stress f

ε° = strain at the ultimate compressive strength f'$_c$

Therefore,

$\varepsilon^\circ = \frac{2*7000}{5072000}$ = 0.00276

$f = \frac{5072000*\varepsilon}{1+(\frac{\varepsilon}{0.00276})^2}$

Using these equations points for stress-strain curve:

Point	Strain (in/in)	Stress (psi)
1	0.000414	2099.8
2	0.0005	2455.4
3	0.001	4483.4
4	0.002	6651.4
5	0.00276	6999.4
6	0.003	7000

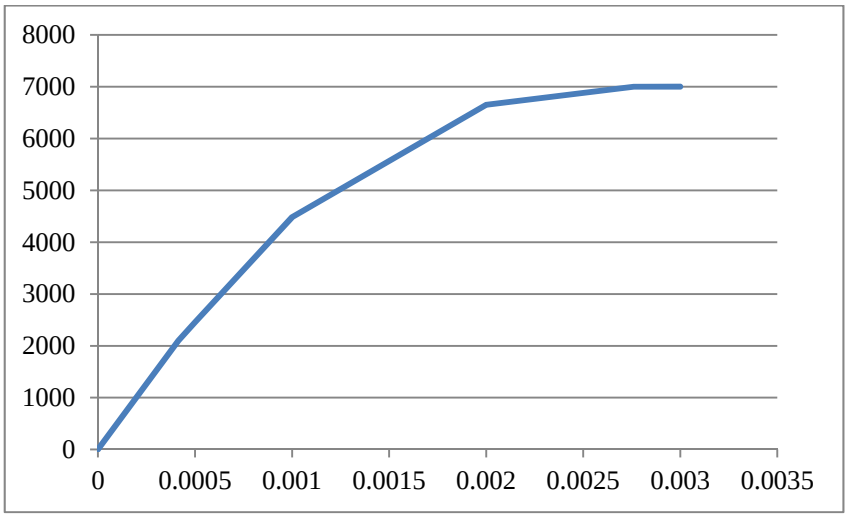

Figure C-1 Uniaxial Stress-Strain Curve for Concrete

C.2 Calculation to Determine Deflection due to Prestress

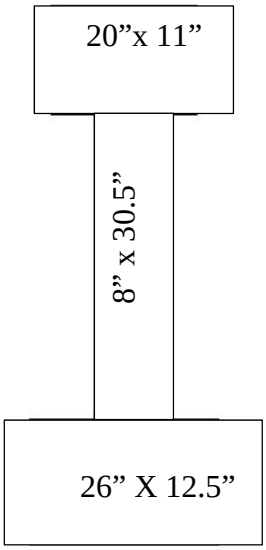

y = 24.68 in

Moment of Inertia of the Cross-section, I_c = 262882.2836 in^4

Modulus of Elasticity of the Concrete, E_c = 5072000 psi

Eccentricity, e = 19.68 in

Span, l = 960 in

Initial Strain of the Prestressed Strand, ε = 0.003571 in/in

Modulus of Elasticity of the Prestressed Strand, E = 28,000,000 psi

Initial Stress of the Prestressed Strand, σ = 0.003571*28,000,000 = 99988 psi

Total Area of the Prestressed Strand, A = 2*2.142 = 4.284 in^2

Total Applied Prestress Load, P = 4.284*99988 = 428348.592 lb

Deflection due to Prestress, $\delta_c = -\frac{Pel^2}{8E_cI_c} = -\frac{428348.592*19.68*960^2}{8*5072000*262882.2836}$ = - 0.7283 in

Area of the cross-section, A_c = 789 in^2

Unit weight of the concrete = 150 pcf

Weight of the prestressed girder, w = $\frac{150*789}{144}$ = 822 plf

Deflection due to self-weight, $\delta_s = \frac{5wl^4}{384E_cI_c} = \frac{5*\left(\frac{0.822}{12}\right)*960^4}{384*12*5072*262882.2836}$ = 0.5682 in

Deflection due to prestress and self-weight, $\delta = \delta_c + \delta_s$ = - 0.7283+0.5682 = - 0.1601 in

C.3 Load at Zero Deflection

$0.1601 = \frac{Pl^3}{48E_cI_c} = \frac{P*960^3}{48*5072000*262882.2836}$

P = 11581 lb

C.4 Load of Application at Decompression

M_t = moment due to self-weight = $\frac{wl^2}{8} = \frac{\left(\frac{822}{12}\right)960^2}{8}$ = 7891200 lb-in

$z_b = \frac{I_c}{y} = \frac{262882.2836}{24.68}$ = 10651.632 in^3

$r = \sqrt{\frac{I_c}{A_c}} = \sqrt{\frac{262882.2836}{789}}$ = 18.253 in

$f_b = -\frac{P}{A_c}\left(1+\frac{ey}{r^2}\right)+\frac{M_t}{Z_b}+\frac{My}{I_c}$

$0 = -\frac{428348.592}{789}\left(1+\frac{19.68*24.68}{18.253^2}\right)+\frac{7891200}{10651.632}+\frac{P*960*24.68}{4*262882.2836}$

P = 26340.80482 lb

C.4 First Cracking Load

$7891200 + \frac{P*960}{4} = 627.5*10651.632 + 428348.592\left(19.68 + \frac{18.253^2}{24.68}\right)$

P = 54188.19446 lb

C.5 Ultimate Flexural Strength

f_{pe} = 99988 psi

f_{pu} = 270000 psi, $0.5f_{pu}$ = 135000 psi

$f_{pe} < 0.5f_{pu}$, Get f_{ps} and c from strain compatibility analysis

$\varepsilon_1 = \varepsilon_{pe} = \frac{f_{pe}}{E_{ps}} = \frac{99988}{28000000}$ = 0.003571

$\varepsilon_2 = \varepsilon_{decompression} = \frac{P}{A_cE_c}\left(1+\frac{e^2}{r^2}\right) = \frac{428348.592}{789*5072000}\left(1+\frac{19.68^2}{18.253^2}\right)$ = 0.000231468

Assume, f_{ps} = 224 ksi

a = $\frac{A_{ps}f_{ps}}{0.85f_c'b} = \frac{4.284*224000}{0.85*7000*20}$ = 8.064 in

β_1 = 0.7

c = $\frac{a}{\beta_1}$ = 11.52 in

d = 49 in

$\varepsilon_3 = \frac{\in_c(d-c)}{c} = \frac{0.003(49-11.52)}{11.52}$ = 0.00976

$\varepsilon_{ps} = \varepsilon_1 + \varepsilon_2 + \varepsilon_3$ = 0.003571 + 0.000231468 + 0.00976 = 0.013563

f_{ps} = 268 - $\frac{0.075}{\in_{ps}-0.0065}$ = 268 - $\frac{0.075}{0.013563-0.0065}$ = 257381.1093 psi

a = 9.2657 in

c = 13.2367 in

$\varepsilon_3 = \frac{\in_c(d-c)}{c} = \frac{0.003(49-13.2367)}{13.2367}$ = 0.008105477

$\varepsilon_{ps} = \varepsilon_1 + \varepsilon_2 + \varepsilon_3$ = 0.003571 + 0.000231468 + 0.008105477 = 0.011908 in/in

f_{ps} = 268 - $\frac{0.075}{\in_{ps}-0.0065}$ = 268 - $\frac{0.075}{0.011908-0.0065}$ = 254131.5166 psi

a = 9.1487 in

c = 13.07 in

$\varepsilon_3 = \frac{\in_c(d-c)}{c} = \frac{0.003(49-13.07)}{13.07}$ = 0.0082472

$\varepsilon_{ps} = \varepsilon_1 + \varepsilon_2 + \varepsilon_3$ = 0.003571 + 0.000231468 + 0.0082472 = 0.01205 in/in

f_{ps} = 254485.7216 psi

$M_n = A_{ps}f_{ps}\left(d_p - \frac{a}{2}\right)$ = 4.284*254485.7216*$\left(49 - \frac{9.1487}{2}\right)$ = 48433591.36 lb-in

P = 201806.6307 lb

C.6 Ultimate Shear Capacity

V_p = 0

M_o = 7891200 lb-in

V_d = 65.76 kip

$f_{pe} = \frac{P_e}{A_c}\left(1 + \frac{ec}{r^2}\right) = \frac{428348.592}{789}\left(1 + \frac{19.68*24.68}{18.253^2}\right)$ = 1334.35 psi

$f_d = \frac{M_o c}{I_c} = \frac{7891200*24.68}{262882.2836}$ = 740.844 psi

$M_{cr} = \left(\frac{I}{y_t}\right)\left(6\sqrt{f_c'} + f_{pe} - f_d\right) = \left(\frac{262882.2836}{29.32}\right)\left(6\sqrt{7000} + 1334.35 - 740.844\right)$

= 9822239.824 lb-in

At mid span, $V_i = \frac{p}{2}$

$M_{max} = \frac{PL}{4}$

$V_{ci} = 0.6\sqrt{f_c'}b_w d + V_d + \frac{V_i M_{cr}}{M_{max}}$

$= 0.6 * \sqrt{7000} * 8 * 49 + 65760 + \frac{p*4*9822239.824}{2*P*960}$

= 105901.2436 lb

$V_{ci,min} = 1.7\sqrt{f_c'}b_w d$ = 55755.02417 lb

$V_{cw} = \left(3.5\sqrt{f_c'} + 0.3f_{pc}\right)b_w d + V_p$

$=\left(3.5\sqrt{7000} + 0.3 * 99988\right) * 8 * 49$

=11873378.56 lb

V_c = min (V_{ci}, V_{cw})

V_c = 105901.2436 lb

$V_s = \frac{A_v f_y d}{s} = \frac{0.22*60000*49}{18.11}$ = 35715.07 lb

$V_n = V_c + V_s$ = 105901.2436 + 35715.07 = 141616.3181 lb

$V_n = \frac{P}{2} + \frac{w_{self} l}{2}$

P = 217472.6362 lb

C.7 Flexural Strengthening

C.7.1 Girder details

Compressive strength of concrete, f'$_c$ = 7000 psi

Ultimate strength of strands = 270 ksi

Number of 0.5 in diameter strands used = 28

Area of girder = 789 in^2

Moment of inertia = 262882.2836 in^4

d_p = 49 in

d_f = 54 in

y_b = 24.68 in

C.7.2 FRP Physical Properties

Thickness, t_f = 0.04 in

Ultimate tensile strength, f_{fu} = 135 ksi

Rupture strain, ε_{fu} = 0.015 in/in

Modulus of elasticity of FRP, E_f = 9000 ksi

C.7.3 Design Steps

Step 1: Calculate the FRP system design material properties

The girder is located in an exterior exposure condition and CFRP material is used. Therefore, per ACI 440 2R, an environmental reduction factor of 0.85 is suggested.

f_{fu} = (0.85)(135) = 114.75 ksi

ε_{fu} = (0.85)(0.015) = 0.01275 in/in

Step 2: Preliminary Calculations

β_1 = 0.7

A_{ps} = 28(0.153) = 4.284 in^2

E_{ps} = 28000 ksi

A_f = 0.04(26) = 1.04 in^2

r = 18.253 in

f_{pe} = 99.988 ksi

ε_{pe} = 0.003571 in/in

P_e = 428.35 ksi

e = 19.68 in

Step 3: Determine the existing state of strain on the soffit

The existing state of strain is calculated assuming the beam is uncracked and the only loads acting on the girder are dead loads.

$\varepsilon_{bi} = -\left[\frac{P_e}{A_c E_c}\left(1+\frac{e y_b}{r^2}\right)+\frac{M_{DL} y_b}{E_c I_g}\right]$

$= -\left[\frac{428348.592}{789*5072000}\left(1+\frac{19.68*24.68}{18.253^2}\right)+\frac{(7891200)\,(24.68)}{(5072000)(262882.2836)}\right]$

= - 0.000117 in/in

Step 4: Determine the design strain of the FRP system

The strain of FRP accounting for debonding failure mode ε_{fd} is calculated

$\varepsilon_{fd} = 0.083\sqrt{\frac{f_c'}{n_f E_f t_f}} \leq 0.9\,\varepsilon_{fu}$

= 0.01157 > 0.011475

ε_{fd} = 0.011475

Because the debonding strain is larger than the rupture strain, debonding does not control the design of the FRP system.

Step 5: Estimate c, the depth of the neutral axis

Assume, c = 12.52 in

Step 6: Determine the efficiency level of strain in the FRP reinforcement

$\varepsilon_{fe} = 0.003\left(\frac{d_f - c}{c}\right) - \varepsilon_{bi} \leq \varepsilon_{fd}$

$\varepsilon_{fe} = 0.003\left(\frac{54-12.52}{12.52}\right)$+0.000117 = 0.01005 < 0.011475

For the neutral axis depth selected, concrete crushing would be the failure mode because the first expression in this equation governed.

Step 7: Calculate the strain in the prestressing steel

$\varepsilon_{pnet} = 0.003\left(\frac{d_p - c}{c}\right)$

$\varepsilon_{pnet} = 0.003\left(\frac{49-12.52}{12.52}\right)$ = 0.00874

$\varepsilon_{ps} = \varepsilon_{pe} + \frac{p_e}{A_c E_c}\left(1 + \frac{e^2}{r^2}\right) + \varepsilon_{pnet} \leq 0.035$

$\varepsilon_{ps} = 0.003571 + 0.000231468 + 0.00874 = 0.01254 < 0.035$

Step 8: Calculate the stress level in the prestressed steel and FRP

$\varepsilon_{ps} > 0.008$

$f_{ps} = 268 - \frac{0.075}{\epsilon_{ps} - 0.0065} = 255.6 < 0.98 f_{pu} = 264.6$

$f_{fe} = E_f \varepsilon_{fe} = 9000 * 0.01005 = 90.45$

Step 9: Calculate the internal force resultants and check equilibrium

For concrete crushing, $\alpha_1 = 0.85$, $\beta_1 = 0.7$

$c = \frac{A_p f_{ps} + A_f f_{fe}}{\alpha_1 f_c' \beta_1 b} = \frac{4.284 * 255.6 + 1.04 * 90.45}{.85 * 7 * .7 * 20} = 14.2744$

Step 10: Adjust c until force equilibrium is satisfied

c = 13.8827

$\varepsilon_{fe} = 0.008786$

$\varepsilon_{pnet} = 0.0075887$

$f_{ps} = 252.67$ ksi

$f_{fe} = 79.074$ ksi

c = 13.9817

Step 11: Calculate design flexural strength of the section

$\varphi M_n = \varphi\left[A_{ps} f_{ps}\left(d_p - \frac{\beta_1 c}{2}\right) + 0.85 A_f f_{fe}\left(d_f - \frac{\beta_1 c}{2}\right)\right]$

$M_n = 4.284 * 252.67\left(49 - \frac{0.7 * 13.9817}{2}\right) + 0.85 * 1.04 * 79.074\left(54 - \frac{0.7 * 13.9817}{2}\right)$

= 51175.07 k-in

P = 213.2295 kip

C.8 Shear Strengthening

C.8.1 Girder details

Compressive strength of concrete, $f'_c = 7000$ psi

Effective beam depth = 54 in

C.8.2 FRP Physical Properties

Thickness, t_f = 0.04 in

Ultimate tensile strength, f_{fu} = 135 ksi

Rupture strain, ε_{fu} = 0.015 in/in

Modulus of elasticity of FRP, E_f = 9000 ksi

C.8.3 Design Steps

Step 1: Calculate the FRP system design material properties

The girder is located in an exterior exposure condition and CFRP material is used. Therefore, per ACI 440 2R, an environmental reduction factor of 0.85 is suggested.

f_{fu} = (0.85)(135) = 114.75 ksi

ε_{fu} = (0.85)(0.015) = 0.01275 in/in

Step 2: Calculate the effective strain level in the FRP shear reinforcement (Considering reinforced concrete)

$L_e = \frac{2500}{(nt_f E_f)^{0.58}}$ = 5.7865

$k_1 = \left(\frac{f_c'}{4000}\right)^{2/3}$ = 1.4522

$k_2 = \left(\frac{d_{fv} - L_e}{d_{fv}}\right) = \frac{38 - 5.7865}{38}$ = 0.8477

$k_v = \frac{k_1 k_2 L_e}{468 \in_{fu}} \leq 0.75$

k_v = 1.193 ≤ 0.75

k_v = 0.75

$\varepsilon_{fe} = k_v \varepsilon_{fu} \leq 0.004$

ε_{fe} = 0.00956 ≤ 0.004

ε_{fe} = 0.004

Step 3: Calculate the contribution of the FRP reinforcement to the shear strength

The area of FRP shear reinforcement, $A_{fv} = 2nt_f w_f$ = 2*1*0.04 = 0.08

The effective stress in the FRP, $f_{fe} = \varepsilon_{fe} E_f$ = .004*9000 = 36 ksi

The shear contribution of the FRP, $V_f = \frac{A_{fv} f_{fe} (sin\alpha + cos\alpha) d_{fv}}{s_f}$ = 0.08*36*38 = 109.44 kip

Step 4: Calculate the shear strength of the section

$\varphi V_n = 0.75(V_c + V_s + 0.85V_f)$

$V_c + V_s$ = 141.616 kip

V_n = 141.616 + 0.85*109.44 = 234.63 kip

$V_n = \frac{P}{2} + \frac{w_{self} l}{2}$

P = 403.5 kip

C.8.4 45 Degree Inclination of the FRP

The shear contribution of the FRP, $V_f = \frac{A_{fv} f_{fe} (sin\alpha + cos\alpha) d_{fv}}{s_f}$ = 0.08*36*38*1.4142

= 154.772 kip

V_n = 141.616 + 0.85*154.772 = 273.1722 kip

$V_n = \frac{P}{2} + \frac{w_{self} l}{2}$

P = 480.6 kip

References

ACI Committee 440. (2008). Guide for the design and construction of externally bonded FRP systems for strengthening concrete structures (Report No. ACI 440.2R-08). Farmington Hills, MI: American Concrete Institute.

American Concrete Institute. (2011). Report on fiber-reinforced polymer (FRP) reinforcement for concrete structures. In ACI Manual of Concrete Practice Part 5-2011. Farmington Hills, MI: Author.

ANSYS. (2012). ANSYS Parametric Design Language (Version 14.5). Canonsburg, PA: ANSYS.

Bakis, C. E., Bank, L. C., Brown, V. L., Cosenza, E., Davalos, J. F., Lesko, J. J., Machida, A., Rizkalla, S. H., & Triantafillou, T. C. (2002). Fiber-reinforced polymer composites for construction state-of-the-art review. Journal of Composites for Construction, 6(2), 73-87.

Cerullo, D., Sennah, K., Azimi, H., Lam, C., Fam, A., & Tharmabala, B. (2013). Experimental study of full-scale pretensioned bridge girder damaged by vehicle impact and repaired with FRP technology. Journal of Composites for Construction, 1-20. doi:10.1061/(ASCE)CC. 1943-5614.0000383

Fanning, P. (2001). Nonlinear models of reinforced and post-tensioned concrete beams. Electronic Journal of Structural Engineering, University College Dublin, Earlsfort Terrace, Dublin 2, Ireland, Sept. 12.

Kachlakev, D., Miller, T., Yim, S., Chansawat, K., & Potisuk, T. (2001). Finite element modeling of reinforced concrete structures strengthened with FRP laminates (Report No. FHWA-OR-RD-01-XX). Salem, OR: Oregon Department of Transportation.

Ludovico, M. D., Prata, A., Manfredi, G., & Cosenza, E. (2010). FRP strengthening of full-scale PC girders. Journal of Composites for Construction, 14(5), 510-520.

MacGregor, J.G. (1992). Reinforced concrete mechanics and design. Englewood Cliffs, NJ: Prentice-Hall, Inc.

Park, S.H., Robertson, I. N., & Riggs, H. R. (2002). A primer for FRP strengthening of structurally deficient bridges (Report No. HWY-L-2001-01). Honolulu, HI: University of Hawaii at Manoa.

Petty, D. A., Barr, P. J., Osborn, G. P., Halling, M. W., & Brackus, T. R. (2011). Carbon fiber retrofit of forty-two-year old AASHTO I-shaped girders. Journal of Composites for Construction, 15(5), 773-781.

Wang, W., Dai, J., & Harries, K. A. (2013). Performance evaluation of RC beams strengthened with an externally bonded FRP system under simulated vehicle loads. Journal of Bridge Engineering, 18(1), 76-82.

Willam, K.J., & Warnke, E.P. (1974). Constitutive model for triaxial behavior of concrete. Seminar on Concrete Structures Subjected to Triaxial Stresses, International Association of Bridge and Structural Engineering Conference, Bergamo, Italy.

Wolanski, A.J. (2004). Flexural behavior of reinforced and prestressed concrete beams using finite element analysis (Unpublished master's thesis). Marquette University, Milwaukee, WI.

Biographical Information

Farzia Haque received her Bachelor of Science in Civil Engineering from Bangladesh University of Engineering and Technology (BUET), Bangladesh in 2011. She started her career as a Structural Engineer at Axis Design Consultants Ltd. She joined University of Texas at Arlington as a graduate student in the Civil Engineering Department in 2012. She started research under Dr. Nur Yazdani in 2013 on the application of the fiber reinforced polymer for bridge strengthening.